

MACHINING STABILITY AND MACHINE TOOL DYNAMICS

**Erhan Budak
Sabanci University
Tuzla, Istanbul
Turkey**

ABSTRACT

Machining is a common manufacturing process in industry due to its high flexibility and ability to produce parts which excellent quality. The productivity and quality in machining operations can be limited by several process constraints one of which is the self-excited chatter vibrations. Under certain conditions, the process may become unstable yielding oscillations with high amplitudes which result in poor surface finish and damage to the cutting tool, part and the machine tool itself. Stability analysis of the dynamic cutting process can be used to determine chatter-free machining conditions with high material removal rate. Since chatter is a result of the dynamic interactions between the process and the structures both cutting and machine tool dynamics are important elements of the stability analysis. In this paper, methods developed for stability analysis of cutting processes and machine tool dynamics will be presented. Implications of these methods in the selection of process parameters and machine tool design will be also discussed with example applications.

Keywords: Machining, machine tool dynamics, chatter stability

1. INTRODUCTION

Machining is one of the most common manufacturing processes in industry due to its ability to produce high quality parts with outstanding flexibility. These characteristics have been further enhanced in last several decades due to the advances in CAM, CNC, machine tool and cutting tool technologies. However, the productivity and quality in machining operations can be limited due to the process mechanics. One of the most common problems in machining is the process instability caused by the chatter vibrations. Under certain conditions, the process may become unstable yielding oscillations with high amplitudes which result in poor surface finish and damage to the cutting tool, part and the machine tool. Stability analysis of the dynamic cutting process can be used to determine chatter-free machining conditions with high material removal rate. In this paper, the analytical methods developed for chatter stability will be presented with applications. In addition, the modeling of the frequency response of machine tool structures will also be demonstrated. The formulations and the applications will be given for turning and milling processes which are the most commonly used machining operations in industry.

Chatter is the result of the dynamic interactions between the cutting process and the machine-tool-part structures. Chatter vibrations develop due to dynamic interactions between the cutting tool and workpiece, and result in poor surface finish and reduced tool life. Tlustý et al. [1] and Tobias [2] identified the most powerful source of self-excitation which is associated with the structural dynamics of the machine tool and the feedback between the subsequent cuts on the same cutting surface resulting in regeneration of waviness on the cutting surfaces, and thus modulation in the chip thickness [3]. Under certain conditions the amplitude of vibrations grows and the cutting system becomes unstable. Although chatter is always associated with vibrations, in fact it is fundamentally due to instability in the cutting system. For a certain cutting speed there is a limiting depth of cut above which the system becomes unstable, and chatter develops. Additional operations, mostly

manual, are required to clean the chatter marks left on the surface. Thus, chatter vibrations result in reduced productivity, increased cost and inconsistent product quality.

Although the basic theory of chatter was developed about five decades ago, the application in industry has been limited due to several reasons. First of all, in most operations the cutting is not orthogonal due to the geometry of the tool and the process. Thus, improved methods are necessary to include the important process parameters in the stability analysis. For example, in the stability analysis of milling the rotating tool, multiple cutting teeth, intermittent cutting action, varying chip load direction and multi-directional dynamics must be considered in the modeling. Similarly, for turning and boring stability, the inclination and side edge cutting angles, and insert nose radius must be included in the analysis. In the early milling stability analysis, Tlustý [3] used his orthogonal cutting model considering an average direction as an approximation. Minis et al. [4, 5] used Floquet's theorem and the Fourier series for the formulation of the milling stability, and numerically solved it using the Nyquist criterion. Budak and Altintas [6, 7] developed a stability method for milling which leads to analytical determination of stability limits. The method was verified by experimental and numerical results, and demonstrated to be very fast for the generation of stability lobe diagrams. More recently, the special case of low immersion milling has been investigated in several studies where added lobes were also presented [8-11]. Kaneko et al. [12] modeled the self excited chatter and chatter marks left on the surface in turning by a 2D model using a numerical solution where the results were mostly based on experimentation. Minis et al. [13], on the other hand, used an oriented transfer function approach where the 3D turning geometry was not fully included into the model. Later, Rao et al. [14] used the multi dimensional approach presented in [7] to model the stability in turning. Atabey et al. [15, 16] proposed an analytical model for force and surface prediction in boring, but the solution was achieved using time domain simulations. In one of the recent works, Budak and Ozlu [17, 18] proposed an analytical stability model for turning and boring operations. The stability model considers the effects of important geometrical parameters such as the rake, inclination and side edge cutting angles and the insert nose radius, and was verified through extensive testing covering different cases.

The other significant part of the chatter stability analysis is the dynamics of the machine tool structure. The frequency response function (FRF), or the transfer function, at the cutting tool-material contact point is required to obtain stability diagrams. Using experimental approach, these FRFs can be obtained directly by impact testing [19]. However, for a different combination of the system components, a new test will be required since the system dynamics will change. Schmitz et al. [20, 21] implemented the well known receptance coupling theory of structural dynamics in order to couple the dynamics of the spindle-holder assembly and the tool by using the dynamical properties at the holder-tool interface. It is suggested that the dynamics of the spindle-holder subassembly can be obtained experimentally at the holder tip for once, then, it can be coupled with the dynamics of the tool which is obtained analytically. In a recent study, Ertürk et al. [22, 23] presented an analytical approach to predict the tool point FRF by modeling the spindle-holder-tool dynamics. They also used the model to analyze the effects of bearing supports and spindle-holder and tool-holder interfaces on the FRF [24], and demonstrated the use of the model in fast and practical generation of the stability diagrams [25].

A common method of chatter suppression is to determine the chatter free cutting conditions, i.e. the cutting depth and speed, through stability analysis or diagrams as described above. However, there are alternative methods of chatter suppression for different applications. One practical method is to use the noise spectrum of the chatter to determine the spindle speeds for higher stability. The dynamic contact between the cutting tool and the work material due to chatter generates high amplitude noise which is one of the undesired results of chatter. However, the spectral analysis of the chatter noise generates a unique opportunity for the detection, and in some cases, suppression of chatter [26-28]. Another alternative method of chatter suppression is the use of variable pitch cutters in milling which may improve the stability significantly [29]. The effectiveness of variable pitch cutters was first demonstrated by Slavicek [30], and then by Opitz et al. [31] and Vanherck [32]. Recently, Altintas et al. [33] adapted the analytical milling stability model to the case of variable pitch cutters. Budak [34] developed an analytical method for the optimal design of variable pitch cutters, and implemented them in the milling of turbine engine impellers and fans made out of titanium alloys [35].

The present paper is organized as follows. The basic orthogonal chatter stability is presented in the next section which is followed by the detailed formulations for turning and milling using multi directional models. After these, the analytical calculation of the FRFs of spindle – tool holder – tool assembly are given. Finally, suppression of chatter using sound spectrum is presented with examples.

2. STABILITY OF ORTHOGONAL CUTTING

In dynamic cutting, a vibrating tool removes a chip from an undulated surface which was generated during the previous pass as shown in Figure 1. The process can be visualized as a superposition of these two distinct mechanisms, i.e. wave removing (outer wave) and wave generation (inner wave). The physics of dynamic cutting can be explained in terms of chip thickness, shear, rake and clearance angle oscillations, and variation of friction forces and flank contact. However, the most important factor for the stability of the process is the regeneration of the chip thickness (h) resulting from the two waves and the phase (ε) between them as shown in Figure 1.

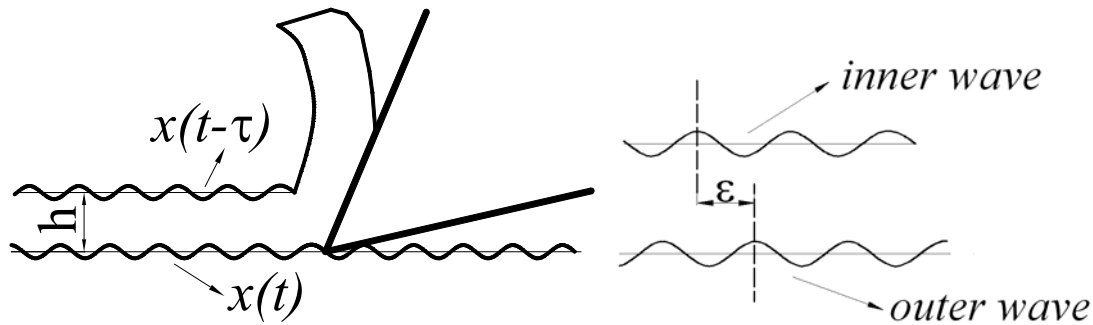


Figure 1. Dynamic chip thickness and regeneration in orthogonal metal cutting

The dynamic cutting force in the feed, or chip thickness, direction can be written as follows:

$$F_f = K_f b h \quad (1)$$

where b is the depth of the cut (in the third direction, i.e. into the plane of paper in Figure 1), h is the instantaneous chip thickness and K_f is the cutting force coefficient in the feed direction which is measured or calibrated through testing [36]. Under the influence of the vibrations, the dynamic chip thickness can be expressed as follows

$$h(t) = h_0 - x(t) + x(t - \tau) \quad (2)$$

where h_0 is the static chip thickness defined by the feed rate of the tool, $x(t)$ and $x(t - \tau)$ are the vibration amplitude in the chip thickness direction during the current and previous passes on the same cut surface, and τ is the time delay between the two waves corresponding to the time to reach to the same position on the surface between two subsequent passes. The dynamic cutting force takes the following form when (2) is substituted in (1)

$$F_f(t) = K_f b [x(t - \tau) - x(t)] \quad (3)$$

The static part of the force due to h_0 has been neglected in (3) as it does not contribute to the regeneration of the chip thickness, and thus the stability of the process. In machining there may be vibrations present due to cutting forces, however if the process is stable their amplitudes are bounded. In general, the vibration amplitude increases exponentially if the system is unstable whereas it decreases exponentially for a stable system. At the stability limit, the amplitude neither increases nor decreases. Thus, at the stability limit the vibration and the dynamic force can be expressed as follows

$$\begin{aligned} x(t) &= X e^{i\omega_c t} \quad , \quad x(t - \tau) = X e^{i\omega_c (t - \tau)} \\ F_f(t) &= F e^{i\omega_c t} \end{aligned} \quad (4)$$

where X and F are the amplitudes of the vibration and the dynamic force, respectively, and ω_c is the vibration, or chatter, frequency. Using the resultant FRF in the chip thickness direction, $G(\omega_c)$, the vibrations can be expressed as

$$X = FG(\omega_c) \quad (5)$$

Substituting (4-5) into (3)

$$Fe^{i\omega_c t} = K_f b G(\omega_c) (e^{-i\omega_c \tau} - 1) Fe^{i\omega_c t} \quad (6)$$

From which the following condition is obtained for the stability limit

$$1 + K_f b G(\omega) (1 - e^{-i\omega_c \tau}) = 0 \quad (7)$$

The exponential term due to the delay can be expressed using trigonometric identities:

$$1 + K_f b (G_R + iG_I) [1 - (\cos \omega_c \tau - i \sin \omega_c \tau)] = 0 \quad (8)$$

where G_R and G_I are the real and imaginary parts of the FRF, respectively. The real and imaginary parts of (8) must be equated to 0 separately:

$$\begin{aligned} K_f b (G_R \sin \omega_c \tau + G_I - G_I \cos \omega_c \tau) &= 0 \\ G_R \sin \omega_c \tau + G_I (1 - \cos \omega_c \tau) &= 0 \end{aligned} \quad (9)$$

The second equation due to the imaginary part of (8) results in the following:

$$\frac{G_I}{G_R} = \frac{\sin \omega_c \tau}{\cos \omega_c \tau - 1} \quad (10)$$

Using the trigonometric identities, the following is obtained:

$$\frac{G_I}{G_R} = \frac{2 \sin(\omega_c \tau / 2) \cos(\omega_c \tau / 2)}{-2 \sin^2(\omega_c \tau / 2)} = -\frac{\cos(\omega_c \tau / 2)}{\sin(\omega_c \tau / 2)} = \tan(-3\pi/2 + \omega_c \tau / 2) \quad (11)$$

Finally, the following condition is obtained

$$2 \tan^{-1} \frac{G_I}{G_R} + 3\pi = \omega_c \tau \quad (12)$$

The number of waves between two subsequent cuts can be described as follows:

$$\omega_c \tau = 2\pi k + \varepsilon \quad (13)$$

Substituting (12) into (13), the following is obtained for the phase

$$\varepsilon = \pi + 2 \tan^{-1} \frac{G_I}{G_R} \quad (14)$$

Thus, for a certain chatter frequency the corresponding phase and the speed (or delay) can be determined from (14) and (13), respectively.

From the first equation of (9) due to the real part of (8), the limiting depth of cut can be obtained as follows:

$$b_{\lim} = \frac{-1}{K_f (G_R - G_R \cos \omega_c \tau - G_I \sin \omega_c \tau)} \quad (15)$$

By reorganizing (15) and substituting (10), the following is obtained:

$$b_{lim} = \frac{-1}{K_f G_R \left(1 - \cos \omega_c \tau - \frac{\sin \omega_c \tau}{\cos \omega_c \tau - 1} \sin \omega_c \tau \right)} \quad (16)$$

Using trigonometric identities again, the following simple equation is obtained for the stability limit:

$$b_{lim} = \frac{-1}{2K_f G_R} \quad (17)$$

Therefore for a given chatter frequency, or speed due to (14), the limiting depth of cut can be predicted using equation (17). For stable cutting, the depth of cut must be lower than b_{lim} in the process. As expected, the stability limit is inversely proportional to the cutting force coefficient and the dynamic flexibility of the system. As G_R is function of the frequency, b_{lim} also varies with the frequency, or with the cutting speed resulting in stability lobes as illustrated in the following sections. The minimum value of the stable depths which is referred to as the absolute stability limit is obtained as follows:

$$b_{lim} = \frac{-1}{2K_f \min(G_R)} \quad (18)$$

The cutting process is stable for all speeds if the depth of cut is lower than the absolute stability limit given by (18).

3. STABILITY OF TURNING PROCESS

The general overview of a turning process is given in Figure 2 where the tool generates cutting action by moving in the feed direction towards the workpiece which rotates around its axis. The surfaces generated in stable and unstable cuts are also shown in Figure 2. It can easily be seen that chatter results in very poor surface quality. In order to formulate the relationship between dynamic turning forces and dynamic chip thickness, all components of the dynamic problem are transformed into the machine axes as shown in Figure 3. From Figure 3 one can deduce that the dynamic displacements in the cutting (z) direction do not affect the dynamic chip thickness. By this observation, the dynamic problem is reduced to a 2D model.

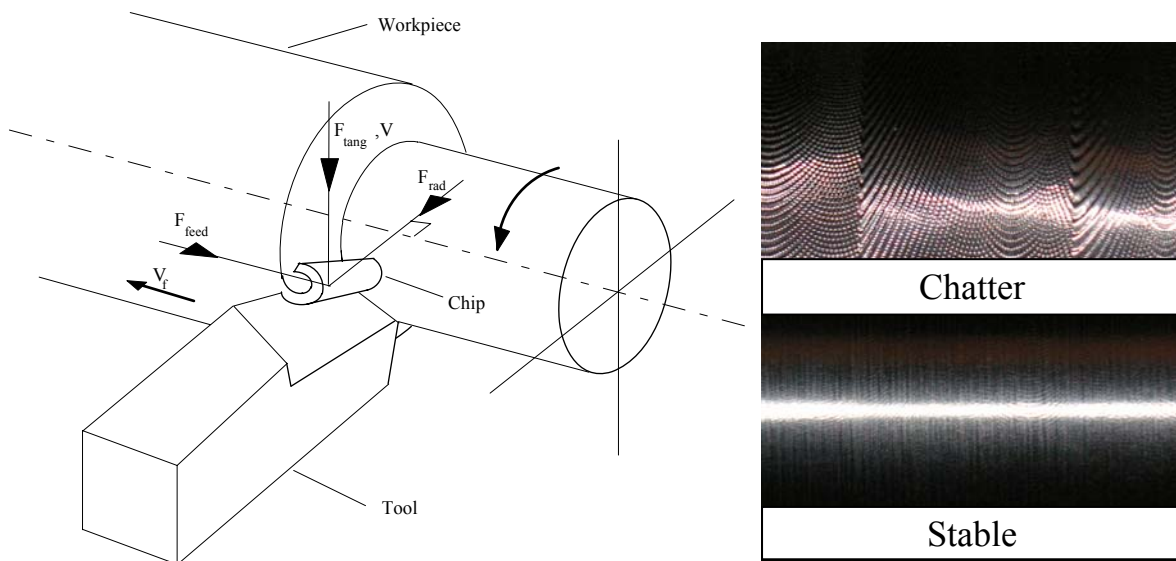


Figure 2. Geometry of turning process and the surfaces generated in stable and unstable cuts.

3.1. Dynamic turning forces

The modulated chip thickness resulting from vibrations of the tool and workpiece can be written as follows [17, 18]:

$$h(t) = f \cos c + \Delta x \cos c - \Delta y \sin c \quad (19)$$

where f represents the feed per revolution, c is the side edge cutting angle, and the dynamic displacement terms are defined as

$$\Delta x = x_c(t) - x_w(t) - x_c(t - \tau) + x_w(t - \tau) \quad (20)$$

$$\Delta y = y_c(t) - y_w(t) - y_c(t - \tau) + y_w(t - \tau)$$

where, $x_c(t)$, $x_w(t)$ and $y_c(t)$, $y_w(t)$ are the cutter and workpiece dynamic displacements for the current pass respectively, and $x_c(t - \tau)$, $x_w(t - \tau)$ and $y_c(t - \tau)$, $y_w(t - \tau)$ are the cutter and workpiece dynamic displacements for the previous pass in x and y directions respectively, and τ is the delay term which is equal to the one spindle revolution period in seconds.

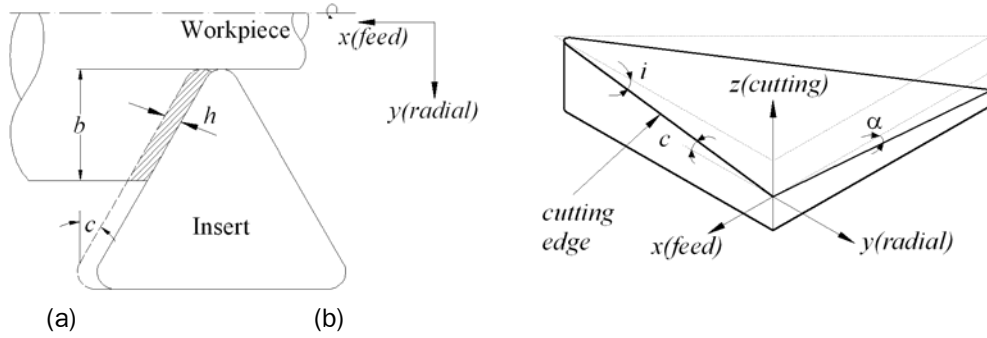


Figure 3. (a) Chip thickness in turning, b) 3D view of the three cutting angles on the insert.

The forces in the feed, F_f , and the radial, F_r , directions contribute to the regeneration whereas the tangential force in the cutting speed direction does not affect the dynamic chip thickness. The dynamic cutting forces on the tool can be expressed as follows:

$$\begin{Bmatrix} F_f \\ F_r \end{Bmatrix} = -\frac{b}{\cos c} \begin{bmatrix} K_f \\ K_r \end{bmatrix} \begin{bmatrix} \cos c & -\sin c \end{bmatrix} \begin{Bmatrix} \Delta x \\ \Delta y \end{Bmatrix} \quad (21)$$

where, K_f and K_r are the corresponding cutting force coefficients and b is the depth of cut. Through coordinate transformation the forces in the x and y directions can be obtained as follows:

$$\{F\} = b[A]\{\Delta d\} \quad (22)$$

where $\{F\}$ is the dynamic force vector containing F_x and F_y and $\{\Delta d\}$ is the dynamic displacement vector both defined in the lathe coordinates. The directional coefficients matrix $[A]$ can be expressed as:

$$[A] = \begin{bmatrix} -\cos c & \sin c \\ \sin c & \cos c \end{bmatrix} \begin{bmatrix} K_f \\ K_r \end{bmatrix} \begin{bmatrix} 1 & -\tan c \end{bmatrix} \quad (23)$$

3.2. Stability limit

Similar to the formulation in Section 2, the response of the cutter and the workpiece at the chatter frequency, ω_c can be expressed as follows:

$$\{d_j(i\omega_c)\} = [G_j(i\omega_c)]\{F\}e^{i\omega_c t} \quad j = c, w ; d = x, y \quad (24)$$

Substituting in (22) considering the delay terms:

$$\{F\}e^{i\omega_c t} = b(1 - e^{-i\omega_c \tau})[A][G(i\omega_c)]\{F\}e^{i\omega_c t} \quad (25)$$

Equation (25) has a non-trivial solution if and only if its determinant is zero, yielding:

$$\det[[I] + \Lambda[G_0(i\omega_c)]] = 0 \quad (26)$$

where $[G_0(i\omega_c)] = [A][G(i\omega_c)]$, and the eigenvalue is defined as $\Lambda = b(e^{-i\omega_c\tau} - 1)$. The solution of Eq. (13) results in the following:

$$\Lambda = 1/[G_{yy}(K_f \sin^2 c \cos c + K_r \sin c \cos^2 c) + G_{xx}(K_f \cos^3 c - K_r \cos^2 c)] \quad (27)$$

Finally, the stability limit, b_{lim} , at a certain chatter frequency can be obtained as follows:

$$b_{lim} = \frac{\Lambda_R + i\Lambda_I}{\cos \omega_c \tau - i \sin \omega_c \tau - 1} \quad (28)$$

Since b is a real number, the imaginary part of Eq. (16) has to vanish yielding:

$$b_{lim} = -\frac{1}{2}\Lambda_R(1 + \kappa^2) \quad (29)$$

where:

$$\kappa = \frac{\Lambda_I}{\Lambda_R} = \frac{\sin \omega_c \tau}{1 - \cos \omega_c \tau} \quad (30)$$

Equation (30) can be used to obtain a relation between the chatter frequency and the spindle speed [7]:

$$\varepsilon = \pi - 2\psi, \quad \psi = \tan^{-1} \kappa \quad (31)$$

$$\omega_c \tau = \varepsilon + 2k\pi, \quad n = 60/\tau \quad (32)$$

where ε is the phase difference between the inner and outer modulations, k is an integer corresponding to the number of waves in a period, and n is the spindle speed in (rpm). The stable depth of cut of the system can be obtained from by equation (29) for different chatter frequencies. These frequencies can be searched around the natural frequency of the most flexible structural mode of the system. Then, the corresponding spindle speeds can be determined from equation (32) for different lobes, i.e. for $k=1,2,3\dots$ etc. Thus, the stability lobe diagram of the dynamic system can be obtained by plotting the stable depth of cut vs. the corresponding spindle speeds for different lobes.

This multi directional turning stability model can also be adapted to the boring process stability as well as to the cases with round inserts or inserts with large nose radii [18]. In those cases, the effective side edge cutting angle varies along the cutting depth resulting in different FRF contributions from the x and y directions, i.e. from the tool and the workpiece. This is handled in [18] by dividing the cutting zone into small elements and combining them in a global matrix equation for the stability. However, since the stable depth of cut is not known in the beginning of the solution, the number of elements to be included in the matrices is not known either. This is solved by following an iterative solution [17, 18].

3.3. Experimental results

The stability lobes in turning and boring operations are very narrow compared to milling stability lobes due to the lower spindle speeds and the single cutting tooth. Thus, chatter tests were conducted in order to obtain the absolute stability limit of the dynamic system experimentally. In the chatter tests, the depths of cut were selected to verify the stable and unstable cutting zones, and absolute stability limit. In order to confirm the absolute stability limit prediction, a fine variation of the depths is used. A conventional manual lathe is used during the experiments, which allows for specific spindle speeds. A modal test setup is used to measure the transfer functions of the workpiece and the tool as shown in Figure 4. The modal test setup consists of an impact hammer, an accelerometer and a data acquisition system. In addition, a sound frequency measurement setup was prepared in order to measure and verify the chatter frequency (Figures 4.c and 4.d). The setup consists of a microphone and a data acquisition setup. As a second check the finished surface is observed by the naked eye for chatter marks in order to verify the unstable cutting operation. The workpiece material used during the tests is a medium carbon steel (AISI 1040), and an existing orthogonal database was used for the cutting force coefficients [36, 19].

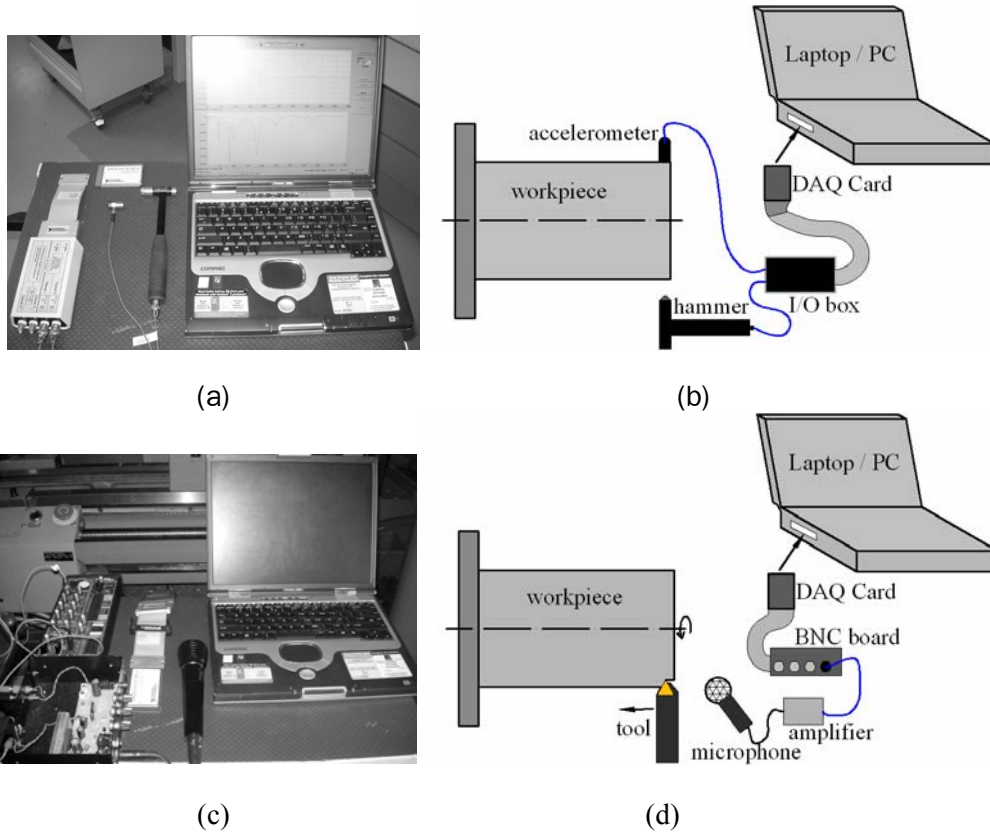


Figure 4. (a), (b) Modal test setup, (c), (d) Frequency measurement setup.

This first set of experiments is conducted in order to verify the proposed stability model for the case where the workpiece is more flexible than the tool. The parameters that are used specifically for the verification of flexible workpiece turning chatter experiments and stability predictions are listed in Table 1 under Case 1. The workpiece diameter and the length were 39 mm and 75 mm, respectively. Moreover, the comparison between the tool and workpiece transfer functions is shown in Figure 5.a.

Table 1: Parameters used in the turning chatter experiments.

	Case 1	Case 2
Side edge cutting angle	30°	25°
Rake angle	5°	5°
Inclination angle	5°	5°
Insert nose radius	0.4mm	varying
Cutting force coefficients, K_f	632 Mpa	632 MPa
Cutting force coefficients, K_r	44 Mpa	44 MPa
Natural frequency of the workpiece	770 Hz	707 Hz
Stiffness of the workpiece	$6.6 \times 10^6 \text{N/m}$	$6.5 \times 10^6 \text{N/m}$
Damping ratio	0.025	0.023

The predicted stability lobes and experimental results are given in Figure 5.c where a sample finished surface after a stable and unstable operation can be seen. Also, the measured chatter sound for 1400 rpm is given in Figure 5.b. Reasonable agreement is observed between the experimental and analytical results.

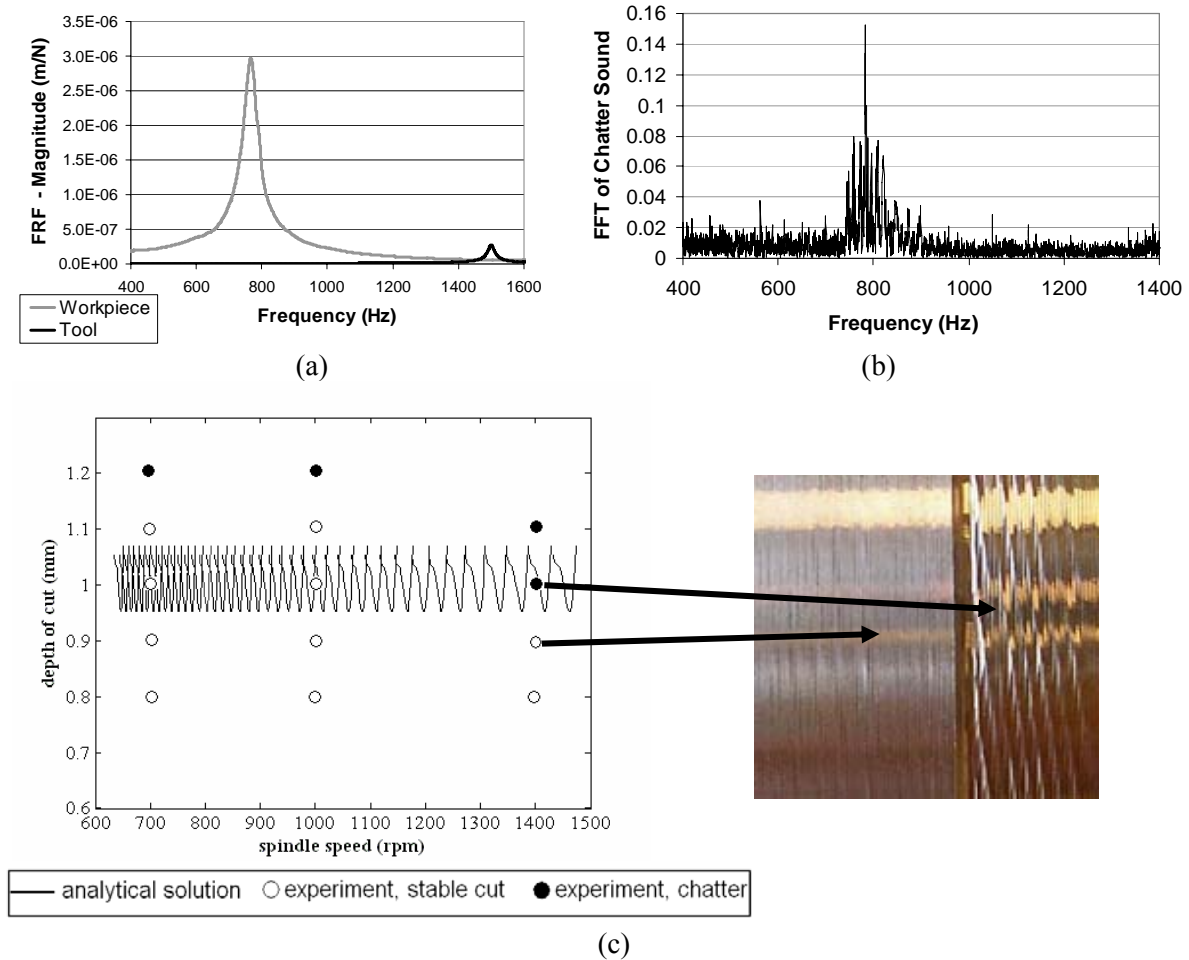


Figure 5. (a) Transfer functions of the tool and the workpiece, (b) chatter sound measurement results for 1400 rpm tests, and (c) chatter test results for model verification and the surface finish of a stable vs. unstable cut.

In the second set of experiments of this case, the effect of the insert nose radius on the stability limit is demonstrated. The cutting conditions and angles used during the chatter tests and the stability predictions are listed in Table 1 under Case 2. The spindle speed used during experiments is 1400 rpm. As in the previous tests, the workpiece diameter was 39 mm and the length was 75 mm.

The analytically predicted stability diagram along with the experimental results is given in Figure 6. As the insert nose radius increases, the effect of workpiece dynamics (which is more flexible) on the chip thickness also increases. Therefore, the dynamic system becomes more flexible resulting in a decrease in the absolute stability limit. In order to explain this situation, firstly it should be noted that when the side edge cutting angle and insert nose radius are zero, the system dynamics are only controlled by the transfer function of the tool in the feed direction. The workpiece dynamics can only affect the dynamics of the cutting system if there is a side edge cutting angle, or the insert has a nose radius. In that case, if the workpiece is more flexible than the tool, the flexibility introduced to the dynamic system reduces the stability limit drastically. Comparing the experimental results and the analytical predictions presented in this section, a close agreement can be concluded.

4. MILLING DYNAMICS AND STABILITY

Milling is a very common process in industry due to its unmatched capability to produce complex 3D surfaces. Dynamics and stability of milling will be presented here with experimental results and applications.

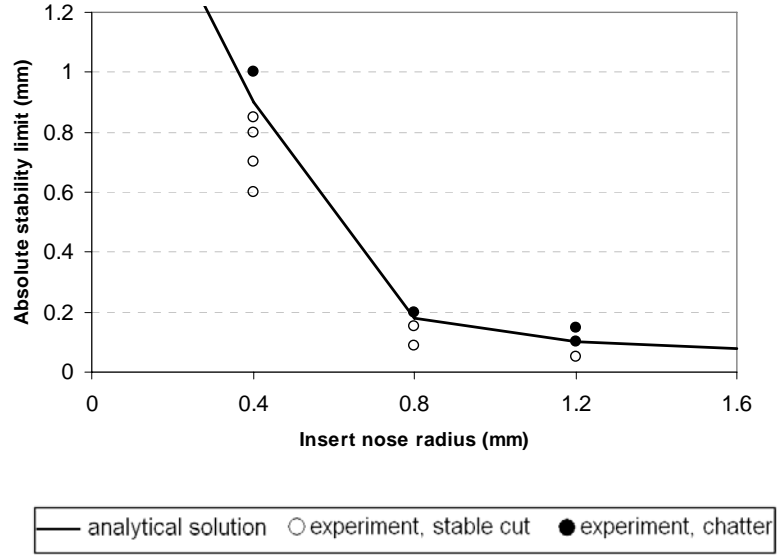


Figure 6. Chatter test results for the case with inserts having different nose radii.

4.1. Dynamic milling forces

The milling cutter and work piece are considered to have two orthogonal modal directions as shown in Figure 7. Milling forces excite both cutter and workpiece causing vibrations which are imprinted on the cutting surface. Each vibrating cutting tooth removes the wavy surface left from the previous tooth resulting in modulated chip thickness which can be expressed as follows:

$$h_j(\phi) = [\Delta x \sin \phi_j + \Delta y \cos \phi_j] \quad (33)$$

where $\phi_j = (j-1)\phi_p + \phi$ is the angular immersion of tooth (j) for a cutter with constant pitch angle $\phi_p = 2\pi/N$ and N teeth. $\phi = \Omega t$ is the angular position of the cutter measured with respect to the first tooth, Ω (rad/sec) being the rotational speed of the tool.

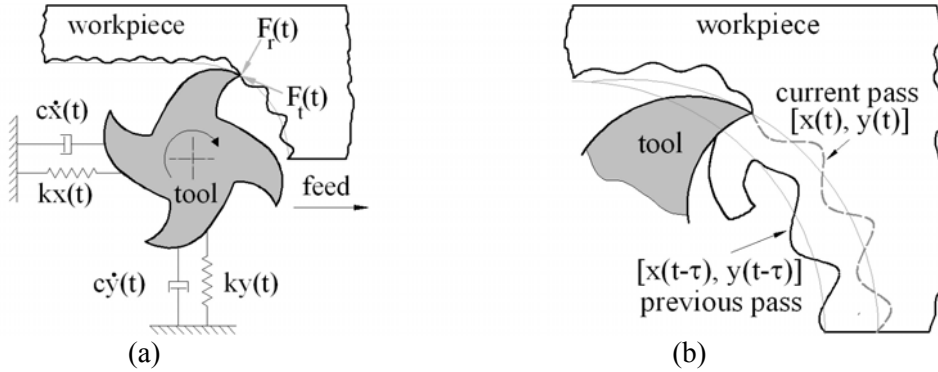


Figure 7. (a) Cross sectional view of an end mill showing regeneration and dynamic forces, and (b) a closer look up to the dynamic chip thickness.

The static part of the chip thickness is neglected in the stability analysis. The dynamic displacements are defined as follows:

$$\begin{aligned} \Delta x &= (x_c - x_c^o) - (x_w - x_w^o) \\ \Delta y &= (y_c - y_c^o) - (y_w - y_w^o) \end{aligned} \quad (34)$$

where (x_c, y_c) and (x_w, y_w) are the dynamic displacements of the cutter and the work piece in the x and y directions, respectively. The superscript (o) denotes the dynamic responses in the previous tooth period which are imprinted on the cut surface. The dynamic cutting forces on tooth (j) in the tangential and the radial directions can be expressed as follows:

$$F_{t_j}(\phi) = K_t a h_j(\phi) \quad ; \quad F_{r_j}(\phi) = K_r F_{t_j}(\phi) \quad (35)$$

where a is the axial depth of cut, and K_t and K_r are the cutting force coefficients which are experimentally identified. After substituting h_j from equation (33) into (35), and summing up the forces on each tooth ($F = \sum F_j$), the dynamic milling forces can be resolved in x and y directions as follows:

$$\begin{Bmatrix} F_x \\ F_y \end{Bmatrix} = \frac{1}{2} a K_t \begin{bmatrix} a_{xx} & a_{xy} \\ a_{yx} & a_{yy} \end{bmatrix} \begin{Bmatrix} \Delta x \\ \Delta y \end{Bmatrix} \quad (36)$$

where α values are the directional coefficients due to the rotation of the tool which makes equation (36) time-varying :

$$\{F(t)\} = \frac{1}{2} a K_t [A(t)] \{\Delta(t)\} \quad (37)$$

$[A(t)]$ is periodic at the tooth passing frequency $\omega = N\Omega$ and with the corresponding period of $T = 2\pi/\omega$. The directional coefficient matrix $[A(t)]$ is periodic at the tooth passing frequency $\omega = N\Omega$ and can be expanded into its Fourier series:

$$[A(t)] = \sum_{r=-\infty}^{r=\infty} [A_r] e^{ir\omega t} \quad ; \quad [A_r] = \frac{1}{T} \int_0^T [A(t)] e^{-ir\omega t} dt \quad (38)$$

Thus, the stability problem has to be solved considering all significant frequencies. Budak and Altintas [7] used two different approaches to the stability solution of milling which will be given separately in the following.

4.2. Stability of dynamic milling-Multi Frequency Solution

If the periodic components of $[A(t)]$ are considered in the solution, then the response of the dynamic forces to these variations should also be included:

$$\{F(t)\} = e^{i\omega_c t} \sum_{k=-\infty}^{\infty} \{F_k\} e^{ik\omega t} = \sum_{k=-\infty}^{\infty} \{F_k\} e^{(\omega_c + k\omega)it} \quad (39)$$

which is equivalent to Floquet's theorem. The dynamic displacements can also be written as follows using the principle of superposition:

$$\{r_p\} = \sum_{k=-\infty}^{\infty} [G_p(i\omega_c + ik\omega)] \{F_k\} e^{(\omega_c + k\omega)it} \quad (p = c, w) \quad (40)$$

$[G_c(i\omega)]$ and $[G_w(i\omega)]$ are the structural transfer function matrices of the cutter and the workpiece. The dynamic displacements for previous and current passes can be expressed as

$$\{r_p^o\} = \{r_p(t-T)\} = e^{-i\omega_c T} \{r_p\} \quad (p = c, w) \quad (41)$$

Substituting into equation (37) the following is obtained:

$$\begin{aligned} \sum_{k=-\infty}^{\infty} \{F_k\} e^{(\omega_c + k\omega)it} &= \frac{1}{2} K_t a (1 - e^{-i\omega_c t}) [A(t)] \sum_{k=-\infty}^{\infty} [G(i\omega_c + ik\omega)] \{F_k\} e^{(\omega_c + k\omega)it} \\ \sum_{k=-\infty}^{\infty} \{F_k\} e^{ik\omega t} &= \frac{1}{2} K_t a (1 - e^{-i\omega_c t}) \sum_{r=-\infty}^{\infty} \sum_{k=-\infty}^{\infty} [A_r] [G(i\omega_c + ik\omega)] \{F_k\} e^{i(r+k)\omega t} \end{aligned} \quad (42)$$

where the total transfer function can be determined by summing tool and workpiece transfer functions., i.e. $[G(i\omega)] = [G_c(i\omega)] + [G_w(i\omega)]$. If both sides of (42) are multiplied by $1/T e^{-ip\omega t}$, and integrated from 0 to T , using the orthogonality principle the following is obtained:

$$\{F_p\} = \frac{1}{2} K_t a (1 - e^{-i\omega_c t}) \sum_{k=-\infty}^{\infty} [A_{p-k}] [G(i\omega + ik\omega)] \{F_k\} \quad (p = 0, \pm 1, \pm 2, \dots) \quad (43)$$

The above equation can be written in an infinite matrix form as:

$$\begin{Bmatrix} \{F_0\} \\ \{F_1\} \\ \{F_{-1}\} \\ \dots \end{Bmatrix} = \frac{1}{2} K_t a (1 - e^{-i\omega_c t}) \begin{bmatrix} [A_0][G(i\omega_c)] & [A_{-1}][G(i\omega_c + i\omega)] & \dots \\ [A_1][G(i\omega_c)] & [A_0][G(i\omega_c + i\omega)] & \dots \\ [A_{-1}][G(i\omega_c)] & [A_{-2}][G(i\omega_c + i\omega)] & \dots \end{bmatrix} \begin{Bmatrix} \{F_0\} \\ \{F_1\} \\ \{F_{-1}\} \\ \dots \end{Bmatrix} \quad (44)$$

Equation (43) has nontrivial solutions if the determinant is zero:

$$\det \left[\delta_{pk} [I] - \frac{1}{2} K_t a (1 - e^{-i\omega_c T}) [A_{p-k}] [G(i\omega_c + ik\omega)] \right] = 0 \quad (45)$$

where δ_{pk} is the Kronecker delta. Equation (45) defines an infinite determinant which is a characteristic of the periodic systems. A truncated version of this equation must be used to obtain approximate solutions. For the first order approximation, $p, k=0, \pm 1$, the following truncated determinant is obtained:

$$\det \begin{bmatrix} [I] + \Lambda [A_0][G(i\omega_c)] & \Lambda [A_{-1}][G(i\omega_c + i\omega)] & \dots \\ [A_1][G(i\omega_c)] & [I] + \Lambda [A_0][G(i\omega_c + i\omega)] & \dots \\ \Lambda [A_{-1}][G(i\omega_c)] & \Lambda [A_{-2}][G(i\omega_c + i\omega)] & \dots \end{bmatrix} \quad (46)$$

where the eigenvalue $\Lambda = -\frac{1}{2} K_t a (1 - e^{-i\omega_c T})$. The Fourier coefficients can be determined by integrating equation (38) in the angular domain,

$$[A_q] = \frac{N}{2\pi} \int_0^T [A(\theta)] e^{-iqN\theta} \quad (47)$$

Resulting in the following

$$\begin{aligned} \alpha_{xx}^{(q)} &= \frac{i}{2} \left[-c_o K_r e^{-iqN\theta} + c_1 e^{-ip_1\theta} - c_2 e^{ip_2\theta} \right]_{\phi_{st}}^{\phi_{ex}} \\ \alpha_{xy}^{(q)} &= \frac{1}{2} \left[-c_o i K_r e^{-iqN\theta} + c_1 e^{-ip_1\theta} + c_2 e^{ip_2\theta} \right]_{\phi_{st}}^{\phi_{ex}} \\ \alpha_{yx}^{(q)} &= \frac{1}{2} \left[c_o K_r e^{-iqN\theta} + c_1 e^{-ip_1\theta} + c_2 e^{ip_2\theta} \right]_{\phi_{st}}^{\phi_{ex}} \\ \alpha_{yy}^{(q)} &= \frac{i}{2} \left[-c_o K_r e^{-iqN\theta} - c_1 e^{-ip_1\theta} + c_2 e^{ip_2\theta} \right]_{\phi_{st}}^{\phi_{ex}} \end{aligned} \quad (48)$$

where

$$\begin{aligned} p_1 &= 2 + Nq \quad , \quad p_2 = 2 - Nq \\ c_o &= \frac{2}{Nq} \quad , \quad c_1 = \frac{K_r - i}{p_1} \quad , \quad c_2 = \frac{K_r + i}{p_2} \end{aligned} \quad (49)$$

4.3. Stability of dynamic milling-Single Frequency Solution

In chatter stability analysis the inclusion of the higher harmonics in the solution may not be required for most cases as the response at the chatter limit is usually dominated with a single chatter frequency. Thus, it is sufficient to include only the average term in the Fourier series expansion of $[A(t)]$ in which case the directional coefficients take the following form:

$$\begin{aligned}\alpha_{xx} &= \frac{1}{2} [\cos 2\phi - 2K_r \phi + K_r \sin 2\phi]_{\phi_{st}}^{\phi_{ex}} ; \quad \alpha_{xy} = \frac{1}{2} [-\sin 2\phi - 2\phi + K_r \cos 2\phi]_{\phi_{st}}^{\phi_{ex}} \\ \alpha_{yx} &= \frac{1}{2} [-\sin 2\phi + 2\phi + K_r \cos 2\phi]_{\phi_{st}}^{\phi_{ex}} ; \quad \alpha_{yy} = \frac{1}{2} [-\cos 2\phi - 2K_r \phi - K_r \sin 2\phi]_{\phi_{st}}^{\phi_{ex}}\end{aligned}\quad (50)$$

Then, equation (37) reduces to the following form:

$$\{F(t)\} = \frac{1}{2} aK_t [A_0] \{\Delta(t)\} \quad (51)$$

By substituting the response and the delay terms in equation (51), the following expression is obtained:

$$\{F\} e^{i\omega_c t} = \frac{1}{2} aK_t (1 - e^{-i\omega_c T}) [A_0] [G(i\omega_c)] \{F\} e^{i\omega_c t} \quad (52)$$

Equation (52) has a non-trivial solution only if its determinant is zero,

$$\det [[I] + \Lambda [G_0(i\omega_c)]] = 0 \quad (53)$$

where $[I]$ is the unit matrix, and the oriented transfer function matrix is defined as:

$$[G_0] = [A_0] [G] \quad (54)$$

and the eigenvalue (Λ) is the same as in multi frequency solution:

$$\Lambda = -\frac{N}{4\pi} K_t a (1 - e^{-i\omega_c T}) \quad (55)$$

4.4. Analytical generation of stability lobes in milling

The chatter stability limit can be determined by solving the characteristic equation of the closed loop milling system. For the single frequency solution, analytical determination of the chatter limit is possible whereas for the multi frequency solution an iterative algorithm needs to be used as both the chatter frequency and the spindle speed, which are dependent, appear in the determinant. Therefore, the formulation for single frequency solution is presented here, however similar procedure can be used for a general solution as it was shown by Merdol and Altintas [37].

If the cross transfer functions, G_{xy} and G_{yx} , in equation (54) are neglected, the eigenvalue can be obtained as flows

$$\Lambda = -\frac{1}{2a_0} \left(a_1 \pm \sqrt{a_1^2 - 4a_0} \right) \quad (56)$$

where

$$\begin{aligned}a_0 &= G_{xx}(i\omega_c) G_{yy}(i\omega_c) (\alpha_{xx} \alpha_{yy} - \alpha_{xy} \alpha_{yx}) \\ a_1 &= \alpha_{xx} G_{xx}(i\omega_c) + \alpha_{yy} G_{yy}(i\omega_c)\end{aligned}\quad (57)$$

Since the transfer functions are complex, Λ will have complex and real parts. However, the axial depth of cut (a) is a real number. Therefore, the complex part of the equation has to vanish yielding

$$\kappa = \frac{\Lambda_I}{\Lambda_R} = \frac{\sin \omega_c T}{1 - \cos \omega_c T} \quad (58)$$

The above can be solved to obtain a relation between the chatter frequency and the spindle speed [7]:

$$\omega_c T = \varepsilon + 2k\pi \quad , \quad \varepsilon = \pi - 2\psi \quad , \quad \psi = \tan^{-1} \kappa \quad , \quad n = \frac{60}{NT} \quad (59)$$

where ε is the phase difference between the inner and outer modulations, k is an integer corresponding to the number of vibration waves within a tooth period, and n is the spindle speed (rpm). After the imaginary part in equation (55) is vanished, the following is obtained for the stability limit:

$$a_{\lim} = -\frac{2\pi\Lambda_R}{NK_t} (1 + \kappa^2) \quad (60)$$

Therefore, for a given cutting geometry, cutting force coefficients, tool and work piece transfer functions, and a chatter frequency ω_c , Λ_1 and Λ_R can be determined from equation (56), and can be used in equations (59) and (60) to determine the corresponding spindle speed and the stability limit. When this procedure is repeated for a range of chatter frequencies and number of vibration waves, k , the stability lobe diagram for a milling system is obtained.

The analytical stability model presented can be used to generate stability lobe diagrams where variation of the stable axial depth of cut with the spindle speed can be shown. Figure 8 shows a sample stability diagram for a milling system analyzed in [38]. As the figure shows, the chatter free material removal rate can be increased substantially by using the high stability pockets. For example, in the first lobe (close to 12 000 rpm), the stability limit is about 5 times the critical (or minimum) stability limit. Note that the stability pockets become larger at higher speeds which is one of the impacts of high speed machining. The figure also shows that the analytical or single frequency solution, multi frequency solution and time domain simulations all converge to the same stability limit for this application.

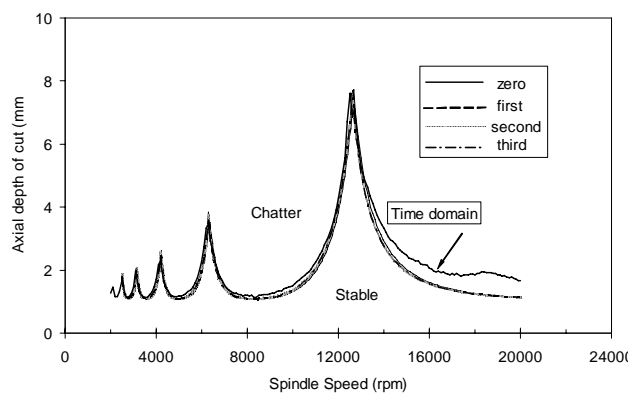


Figure 8. A sample stability diagram for a milling application.

As a second example, a case considered by Merdol and Altintas [37] is presented where the stability diagram is given in Figure 9. In this case, the stability of a very low radial immersion milling is analyzed. For those cases, the predictions of the single frequency solution may not be as accurate. This is mainly because of the increased Fourier series content in the directional coefficients, and thus in matrix $[A]$, due to very short contact between the tool and the material resulting in a very short pulse-width waveform. Thus, higher harmonics in the Fourier series need to be included, and the truncated version of (46) must include more terms. As a result, many different combinations of the tooth frequency and the chatter frequency affect the system response, i.e. $G(ik\omega \pm \omega_c)$, resulting in deviations from the single frequency solution. The stability diagram shown in Figure 9 demonstrates one major deviation from the single frequency solution, i.e. the added lobe which occurs only for very small radial immersion cases. However, the multi frequency solution is able to predict this phenomenon precisely.

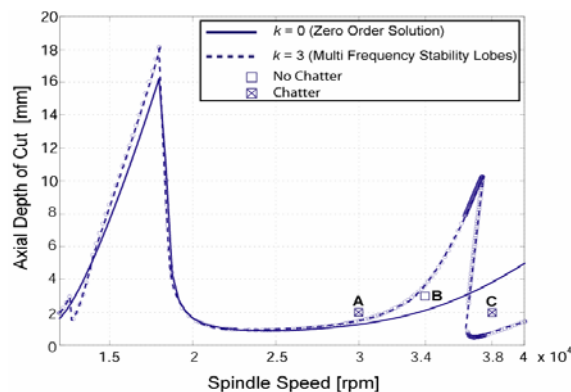


Figure 9. Stability diagram for a low radial immersion application.

4.5. Chatter suppression using variable pitch end mills

Variable pitch cutters have non uniform pitch spacing between the cutting teeth and may be very effective suppressing chatter. The non uniform pitch may disturb the regeneration mechanism, and if the angles selected appropriately the phase between the inner and outer modulation can be minimized. The fundamental difference in the stability analysis of milling cutters with non-constant pitch angle is that the phase delay is different for each tooth:

$$\varepsilon_j = \omega_c T_j \quad (j = 1, \dots, N) \quad (61)$$

where T_j is the j^{th} tooth period corresponding to the pitch angle ϕ_{pj} . The dynamic chip thickness and the cutting force relations given for the standard milling cutters apply to the variable pitch cutters, as well. The eigenvalue expression will take the following form due to the varying phase:

$$\Lambda = \frac{a}{4\pi} K_t \sum_{j=1}^N \left(1 - e^{-i\omega_c T_j} \right) \quad (62)$$

The stability limit can be obtained from equation (62) as:

$$a_{\text{lim}}^{yp} = -\frac{4\pi}{K_t} \frac{\Lambda}{N - C + iS} \quad (63)$$

where

$$C = \sum_{j=1}^N \cos \omega_c T_j \quad ; \quad S = \sum_{j=1}^N \sin \omega_c T_j \quad (64)$$

As a_{lim} is a real number, the imaginary part of equation (63) must vanish yielding [34]

$$a_{\text{lim}}^{yp} = -\frac{4\pi}{K_t} \frac{\Lambda_I}{S} \quad (65)$$

The optimization of pitch angles for a given milling system has more practical importance than the stability analysis for an arbitrary variable pitch cutter. Equation (65) indicates that in order to maximize the stability limit, $|S|$ has to be minimized. From equation (64), S can be expressed as follows:

$$S = \sin \varepsilon_1 + \sin \varepsilon_2 + \sin \varepsilon_3 + \dots \quad (66)$$

where $\varepsilon_j = \omega_c T_j$. The phase angle, which is different for every tooth due to the non-constant pitch, can be expressed as follows:

$$\varepsilon_j = \varepsilon_1 + \Delta\varepsilon_j \quad (j = 2, \dots, N) \quad (67)$$

where $\Delta\varepsilon_j$ is the phase difference between tooth j and tooth (1) corresponding to the difference in the pitch angles between these teeth. The pitch angle variation ΔP corresponding to $\Delta\varepsilon$ can be determined as:

$$\Delta P = \frac{\Delta\varepsilon}{2\pi} \theta = \frac{\Omega}{\omega_c} \Delta\varepsilon \quad (68)$$

There are many solutions to the minimization of $|S|$, i.e. ($S=0$). It can be found out by intuition that $S=0$ for the following conditions [34]

$$\Delta\varepsilon = k \frac{2\pi}{N} \quad (k = 1, 2, \dots, N-1) \quad (69)$$

The corresponding ΔP can be determined using equation (68).

The increase of the stability with variable pitch cutters over the standard end mills can be determined by considering the ratio of stability limits. For simplicity, the absolute or critical stability limit for

equal pitch cutters, i.e. the minimum stable depth of cut regardless of the spindle speed, are considered. The absolute stability limit is the minimum stable depth of cut without the effect of lobing which can be expressed as follows:

$$a_{cr} = -\frac{4\pi\Lambda_I}{NK_t} \quad (70)$$

Then, the stability gain can be expressed as

$$r = \frac{a_{lim}^{vp}}{a_{cr}} = \frac{N}{S} \quad (71)$$

r is plotted as a function of $\Delta\varepsilon$ in Figure 10. for a 4-tooth milling cutter with linear pitch variation. The phase ε depends on the chatter frequency, spindle speed and the eigenvalue of the characteristic equation. Therefore, the stability analysis has to be performed for the given conditions. Three different curves corresponding to different ε_1 values are shown in Figure 10 to demonstrate the effect of phase variation on r . r is maximized for integer multiples of $2\pi/N$, i.e. for $(1/4, 1/2, 3/4)\times 2\pi$. $\Delta\varepsilon+k2\pi$ ($k=1, 2, 3, \dots$) are also optimal solutions, however, they result in higher pitch variations which is not desired.

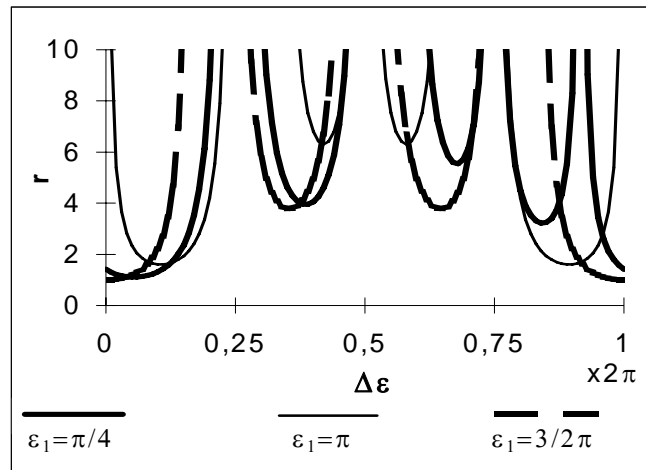


Figure 10. Effect of ε_1 on stability gain for a 4-fluted end mill with linear pitch variation.

5. MACHINE TOOL DYNAMICS

Dynamic rigidity is one of the most critical characteristics of machine tools especially for high precision and high performance machining applications. It determines the dynamic response of the machine structure to cutting forces and inertial loads during the acceleration and the deceleration of the axes. High amplitude vibrations in response to these loads may result in poor machined part quality and potential damage to the machine. A machine tool's dynamic rigidity depends on many factors such as its configuration, size, construction method etc. The overall dynamic rigidity in a machining system depends on all of the components involved, i.e. machine tool, tooling, fixtures, workpiece etc. Therefore, the rigidity of all components in a machining system is critical as the one with the lowest rigidity usually determines the rigidity of the whole system.

Machine tool vibrations exhibit some special characteristics compared to other machinery. The most important type of machine tool vibrations, chatter, is a result of the interaction between the cutting process and the machine structure. It must be noted that chatter may develop even if there is no external periodic excitation. Thus, chatter is a self-excited vibration type which develops at one of the natural modes of the structures, normally the most flexible one at the point of contact between the cutting tool and the work material. Therefore, the dynamic rigidity, which can be represented by the receptance or frequency response function of the structure at the point of interest, is the fundamental information to be used in the machine tool dynamics and chatter stability analyses. This is different

than most other structural analysis applications where the focus is mainly on the modal frequencies in order to predict and avoid the resonance. In the analysis of machine tool dynamics, the amplitude of the dynamic response is the most relevant and important information. In this section, important aspects of experimental methods will be reviewed, and a novel analytical method based on structural dynamics methods for machine tool dynamics modeling will be presented.

5.1. Experimental methods

Dynamic testing has been the most common method of machine tool dynamic analysis. The frequency response function (FRF) or the Transfer Function (TF) can be generated using several experimental methods. The main idea is to excite the structure at a certain frequency and location, and determine its dynamic response at the same or a different point. When this is repeated for a range of frequencies, the frequency response or the transfer function at the relevant point is obtained. The excitation to the structure can be provided by an electromagnetic or hydraulic shaker where its tip is fastened to the point of interest. Although the response can be measured by many different sensor types such as displacement or velocity transducers, the most common method is to use accelerometers. As the shaker generates a harmonic force at a certain frequency both force and the response signals are recorded. Then, the frequency response at this particular frequency can be directly determined from the ratio of the response amplitude to the force amplitude. The phase information can also be obtained from the recorded data. Although the data processing part is quite straightforward, this method has several disadvantages. First of all, the shaker can be a costly instrument compared to other alternatives. Also, it needs to be fastened to the structure which requires some sort of permanent modification such as drilling and threading a hole. Furthermore, the test can be quite time consuming as it needs to be repeated for many frequencies in the range of interest.

A more practical approach is to use Fourier analysis where an impulsive force instead of a harmonic one can be used to excite a wide range of frequencies in one test. This can be done since theoretically an ideal impulse function with infinitesimal impulse period, i.e. 0^+ , contains infinite number of frequencies which can be shown by Fourier analysis. Thus, the idea is to use the Fourier transform of input and output signals to determine the entire frequency response function in one test. This approach has been commonly used in impact tests where a point on the structure is excited using an instrumented hammer and the response at the same or another point is measured by a sensor, usually an accelerometer. A schematic view of a typical impact test set-up is shown Figure 11. The impact hammer is instrumented with a force sensor to capture the applied impact force. Piezoelectric crystals are commonly used sensor types for the force and acceleration measurements, and they may need charge amplification before the data can be acquired by a computer through analogue to digital conversion. It should be noted that an accelerometer with a large mass will affect the dynamics of the structure due to the added mass yielding erroneous measurements whereas a very small accelerometer may not have the required sensitivity especially in the low frequency range. The hammer size and its tip geometry are other important decisions in the dynamic tests. The hammer size and the tip must be selected properly to provide sufficient excitation to the structure for the required frequency range.

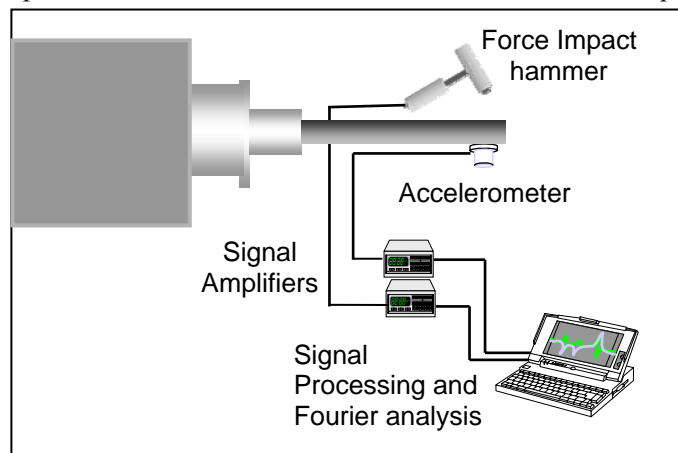


Figure 11. Impact test sup-up used for frequency response measurements.

In order to obtain the FRF, the measured input and the output are transferred to the frequency domain using the Fourier analysis. As a result, the TF between the response measurement point (i) and the force application point (j) can be obtained as follows:

$$G_{ij}(\omega) = \frac{X_i(\omega)}{F_j(\omega)} \quad (72)$$

When the response and the excitation at the same point (i) are considered, then the direct FRF at this point is obtained. Note that since usually the transfer function in terms of displacement, X , is needed in the dynamic analysis, the accelerometer signal needs to be integrated. In general, in an FRF there can be contributions of many structural modes of the measured structure. Therefore, for a general case, multi mode identification methods using curve fitting and error minimization techniques must be used. However, for most structures these modes are well separated, and only a couple of modes (sometimes even just one) dominate the dynamic response of the structure at the point of interest.

Although for chatter stability analysis only the transfer function at the tool tip is required, the measurements at different points, and between different points, should be performed to determine the full dynamic behaviour of the machine tool. By performing the impact test at different points either by moving the response or the impact points the FRF matrix, $[G]$, can be obtained where:

$$\{X\} = [G]\{F\} \quad (73)$$

The FRF matrix is also useful to determine the mode shapes. In many cases it is necessary to determine the component which is responsible for vibrations. This cannot be determined through a single FRF measurement whereas it can easily be identified from mode shapes. If for example, the excitation is given at point 1, the amplitudes of G_{11} , G_{12} , G_{13} etc. at the first resonance peak can be used to determine the first mode shape, and in the second peak for the second mode shape etc. Figure 12 shows the mode shapes of tool assembly on a horizontal machining center. The assembly includes a long tool adapter which is necessary for accessibility to deep pockets on the part but makes the system very flexible. As it can be seen from the figure, the first mode (260 Hz) is the spindle mode as the displacement in the rest of the assembly is relatively small. The second and the third modes belong to the holder and the adapter, respectively. The last mode shown at 5740 Hz is the tool mode where the elastic displacement of the tool can be clearly seen.

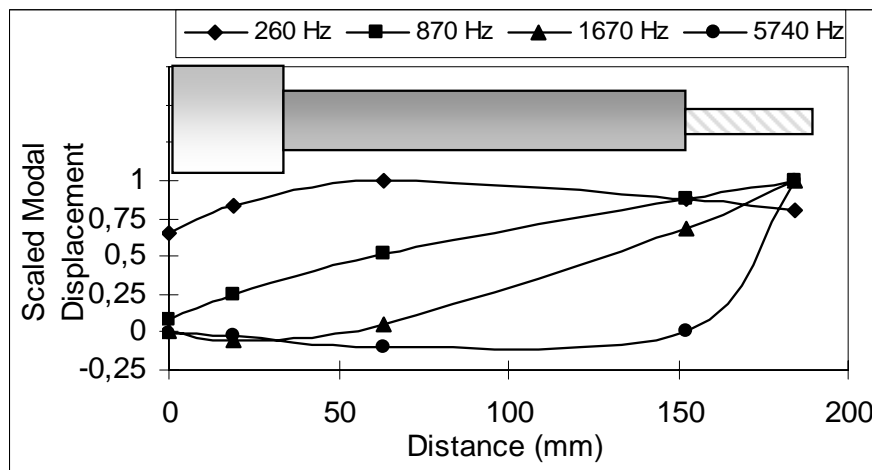


Figure 12. Mode shapes of a tool assembly on a horizontal machining center.

5.2. Analytical modeling of machine tool dynamics

The use of experimental modal analysis may not be very practical always especially for production applications where many combinations are possible. In order to reduce experimentation, the receptance coupling theory of structural dynamics can be used [20-25]. This method is based on the coupling of component dynamics analytically, and can be used effectively for modeling dynamics of complex structures provided that the component dynamics are known.

Ertürk et al. [22-25] presented an analytical model to predict the tool point FRF by modeling all components of the spindle-holder-tool assembly analytically. They used Timoshenko beam theory, receptance coupling and structural modification techniques. Due to the high length to diameter ratios of many spindle and tool sections, Euler-Bernoulli beam model may result in considerable errors in prediction of modal frequencies which is significantly improved using Timoshenko beam formulation. Spindle, holder and tool are modeled as multi-segment beams by using Timoshenko beam theory. The individual multi-segment components are formed by coupling the end point receptances of uniform beams rigidly. Determination of the end point receptances of a uniform Timoshenko beam with free end conditions is given in [22] in detail. The end point receptance matrix of a beam A can be represented as

$$[A] = \begin{bmatrix} [A_{11}] & [A_{12}] \\ [A_{21}] & [A_{22}] \end{bmatrix} \quad (74)$$

where sub matrices of the above matrix include the point and transfer receptance functions of the segment end points (1) and (2). For example, the point receptance matrix of node $A1$ in beam A is given as

$$[A_{11}] = \begin{bmatrix} H_{A1A1} & L_{A1A1} \\ N_{A1A1} & P_{A1A1} \end{bmatrix} \quad (75)$$

The receptance functions, which are denoted by letters H , N , L and P , are defined as follows:

$$\begin{aligned} y_j &= H_{jk} \cdot f_k & \theta_j &= N_{jk} \cdot f_k \\ y_j &= L_{jk} \cdot m_k & \theta_j &= P_{jk} \cdot m_k \end{aligned} \quad (76)$$

where y and θ represent the linear and angular displacements, respectively, and f and m are the forces and the moments, respectively, at the points i and j . Two beams, A and B , can be coupled dynamically using rigid receptance coupling and the receptance matrix of resulting two-segment beam C can be obtained as follows:

$$[C] = \begin{bmatrix} [C_{11}] & [C_{12}] \\ [C_{21}] & [C_{22}] \end{bmatrix} \quad (77)$$

where

$$\begin{aligned} [C_{11}] &= [A_{11}] - [A_{12}] \cdot \left([A_{22}] + [B_{11}] \right)^{-1} \cdot [A_{21}] \\ [C_{12}] &= [A_{12}] \cdot \left([A_{22}] + [B_{11}] \right)^{-1} \cdot [B_{12}] \\ [C_{21}] &= [B_{21}] \cdot \left([A_{22}] + [B_{11}] \right)^{-1} \cdot [A_{21}] \\ [C_{22}] &= [B_{22}] - [B_{21}] \cdot \left([A_{22}] + [B_{11}] \right)^{-1} \cdot [B_{12}] \end{aligned} \quad (78)$$

By following the same formulation, one might continue coupling more segments like a chain to form an n -segment beam. In order to include the dynamics of bearings, A structural modification technique presented by can be used as shown in detail in [22]. In this case, the dynamic structural modification matrix represents the translational and rotational, stiffness and damping information of the bearings. The final step is to couple the main system components to obtain the tool point FRF. However, these components should be coupled elastically due to the flexibility and damping at the contacts. When the end point receptances of the spindle on bearings (S) are coupled with those of the holder (H), the end point receptance matrices of the spindle-holder assembly (SH) can be obtained from:

$$[SH_{11}] = [H_{11}] - [H_{12}] \left[[H_{22}] + [K_{sh}]^{-1} + [S_{11}] \right]^{-1} [H_{21}] \quad (79)$$

$[K_{sh}]$ is the complex stiffness matrix representing the spindle-holder interface dynamics. Note that the receptance matrix $[SH_{11}]$ is very similar to $[C_{11}]$ given in equation (78) with the addition of $[K_{sh}]^{-1}$ only. Finally, the tool (T) can be added to the spindle-holder (SH) system to obtain the end point FRFs of spindle-holder-tool (SHT) assembly. The FRF required for the stability lobe diagram of a given spindle-holder-tool assembly is the one that gives the relation between the transverse displacement and force at the tool tip, which is the first element of the following

$$[SHT_{11}] = [T_{11}] - [T_{12}] \left[[T_{22}] + [K_{ht}]^{-1} + [SH_{11}] \right]^{-1} [T_{21}] \quad (80)$$

As an example application, consider the geometry of the spindle-holder-tool combination shown in Figure 13. Each of the system components, i.e. spindle, holder and tool are composed of several sections with different diameter and lengths which are modeled as multi-segment beams. The dimensions of the components, bearing and interface dynamical properties are given [22]. In order to verify the results of the model, the vibration modes of this assembly were calculated using the finite element method using ANSYS® 9.0. The beam element, which is based on Timoshenko beam theory, is used by restricting the degrees of freedom other than motion in one transverse direction and flexural rotation so that the finite element model is consistent with the model. The natural frequencies obtained by the analytical model and the finite element solution are tabulated in Table 2. As can be seen from the table, the natural frequencies of the assembly obtained by the model presented in this paper and those obtained by using the finite element software are in good agreement and the maximum difference observed for the first seven modes is about 5 %.

Table 2. Natural frequencies of the assembly.

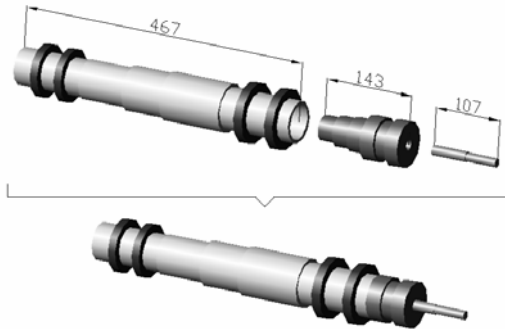


Figure 13. Components of the assembly used in the example.

Mode	Model [Hz]	FEA [Hz]	Diff. [%]
1	71.7	71.6	0.14
2	195	193.8	0.62
3	877.8	867.5	1.19
4	1438.3	1424.3	0.98
5	1819.5	1752.6	3.82
6	3639.3	3442.5	5.72
7	3812.5	3634.8	4.89

5.3. Interface parameters

One important element of machine tool dynamics modeling, or the receptance coupling method in general, is the connection parameters between the components. They may affect the overall response, however there is no accurate modeling methods to predict them. Even experimental identification of these parameters can be quite challenging due to the existence of many unknown parameters in an assembly. However, this task can be simplified by analyzing the effects of parameters in each individual connection on the total response. It was observed [24] that the dynamics of the front bearings primarily control the first rigid body mode whereas the rear bearings mainly affect the second rigid body mode. This also implies that if chatter develops in one of the first two modes, changing the holder or the tool may not help. It is also observed that the translational stiffness at the spindle-holder interface dominantly affects the first elastic mode of the FRF. Furthermore, the rotational stiffness at the same interface has almost negligible effect on the FRF [24]. A similar analysis is performed in order to study the sensitivity of FRF to the holder-tool interface dynamics. It

is observed that the translational stiffness strongly controls the second elastic mode. Similar to the spindle-holder interface, the rotational stiffness at this connection has negligible effect on FRF. Therefore, the observations made so far indicate that, for the first elastic mode, spindle-holder interface is the most important link in the chain, whereas the same is true for holder-tool interface for the second elastic mode in this case study. The connection damping values have similar effects, but on the FRFs peak amplitudes instead of the frequencies. For example, it is observed that the front bearing damping affects the FRF values at the first rigid body mode, translational contact damping at the spindle-holder interface mainly alters the peak value of the first elastic mode etc. [24].

5.4. Example case

A BT40 type holder in which a carbide tool of 12.7mm diameter and 175mm length is inserted with an overhang length of 74 mm is assembled to the free spindle shown in Figure 14. The measured FRF and the model simulation of the tool point FRF are given in Figure 15. The interface parameters were identified experimentally [23]. The agreement between the measured and the predicted FRF can be considered as satisfactory.



Figure 14. Spindle suspended for free-free measurements.

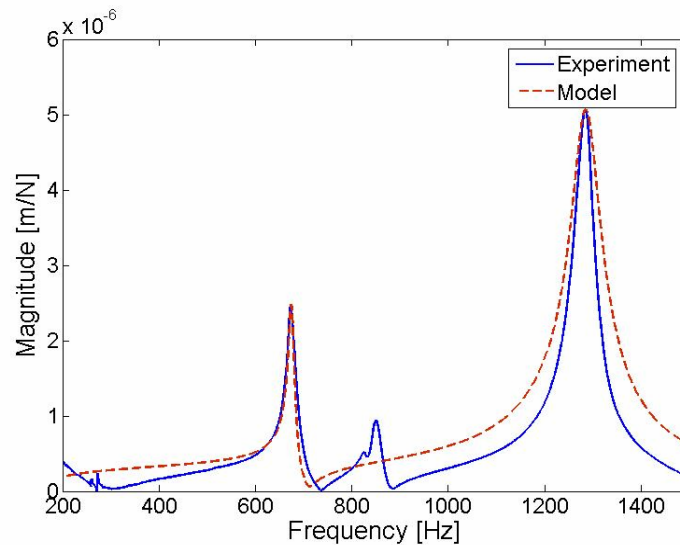


Figure 15. Measured and predicted tool point FRF of the assembly.

5.5. Application to chatter suppression

The analytical machine tool dynamics model presented can be effectively used in chatter suppression which is presented in this section. An SK40 type holder, in which a 4-teeth HSS tool of 110.7 mm length and 12 mm diameter is inserted, is assembled to the 5-axis machining center shown in Figure 16. Tool point FRF of the assembly is measured by impact test at the tool tip using a low mass accelerometer and an instrumented hammer. It is aimed in this section to predict the variations in the resulting FRF for different overhang lengths in order to improve chatter stability by selection of the tool length. The predictions are compared with experimental results for the verification of the approach employed. The translational

interface dynamic parameters are identified by following the approach suggested in [24] using the experimental results for $L=60$ mm. The average values given in the literature are used for the rotational dynamic parameters at spindle-holder and holder-tool connections, since the required FRF values are insensitive to these values as concluded in the above referred paper. The experimentally obtained tool point FRF and the model prediction for $L=60$ mm for are shown in Figure 16.b.

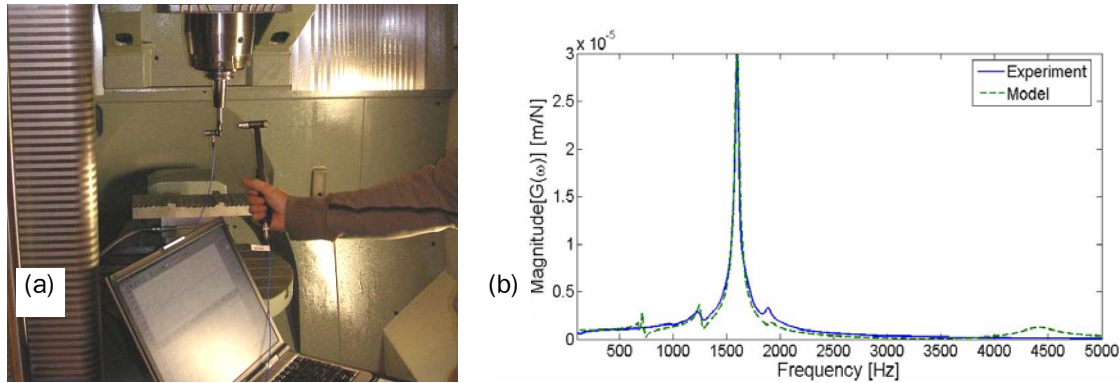


Figure 16. (a) 5-axis machining center with the experimental modal analysis setup and (b) measured and predicted tool point FRF for the overhang length $L=60$ mm.

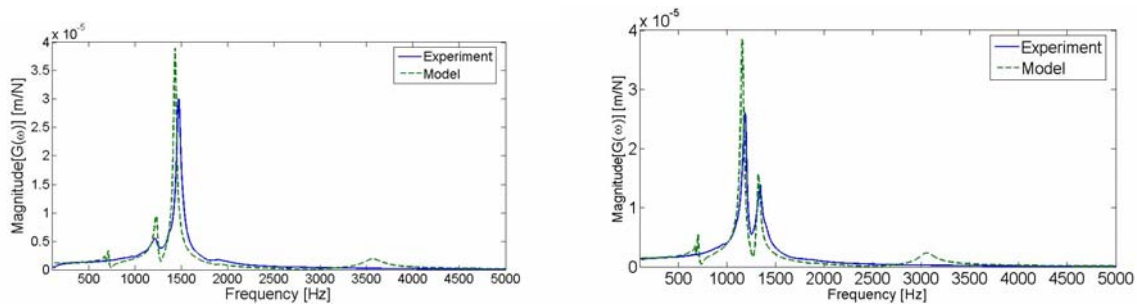


Figure 17. Experimental and predicted tool point FRF; (a) 70 mm overhang length and (b) 80 mm overhang length

The dominant mode appearing at 1594 Hz is the tool mode, and thus its frequency can simply be altered by changing the overhang length of the tool. Overhang length of the tool is changed from 60 mm to 80 mm with an increment of 10 mm while keeping the clamping torque constant at 40 N.m. It is assumed that holder-tool interface dynamic parameters do not change with changing overhang length. Figure 17a and 17b show the predicted and measured tool point FRFs for 70 mm and 80 mm tool overhang lengths, respectively. Note that, accurate knowledge of the variation in contact dynamics (especially damping) with tool overhang length would certainly improve the accuracy of the FRF predictions. That is, a mathematical model for contact stiffness and damping, or a methodology which provides this information for different clamping lengths, torques and tool types by using a limited set of experiments would yield more accurate theoretical results for FRF predictions. As the overhang length of the tool is increased to 70 mm, the tool mode approaches to the small amplitude spindle mode seen around 1220 Hz, which slightly increases amplitude of the latter. Further increase in the tool overhang length (to 80 mm) brings the tool mode closer to the spindle mode and reduces the amplitude of the tool vibrations in a favorable manner as can be seen in Figure 17b. The interaction between two modes reduces not only the frequency, but also the amplitude of vibrations. As a consequence, if this mode interaction can be realized in practical applications, higher depths of cut can be obtained at lower cutting speeds. In order to make use of this effect in practice, one should first identify the tool mode from the FRF, and then alter its frequency towards a close and relatively stationary spindle mode by changing the tool overhang length until the mode is split and vibration amplitude is reduced.

The application of the presented FRF prediction method in chatter stability analysis has also been investigated. A series of tests have been conducted on an aluminum test piece. First, the cutting force

coefficients were identified using milling tests and linear-edge force model [36]. The 4-teeth HSS end mill with 12 mm diameter and 30° helix angle mentioned above was used in down milling mode where the radial depth of cut was 3 mm. The tangential and the radial cutting force coefficients were obtained as $K_t = 550$ MPa and $K_r = 110$ MPa. First of all, the stability diagram was generated for the case of 60 mm tool overhang length (Figure 17) using the analytical milling stability model [7]. The experimentally obtained chatter stability limits at certain spindle speeds are also shown in Figure 18. All cutting tests were performed on a high speed machining center. The instability condition was identified using the spectrum analysis of the sound measurements during cutting. Considering a wide speed range which results in variation in the force coefficients (the average values were used) and narrow stability pockets due to low damping, the agreement between the experimental and the analytical results can be considered as satisfactory.

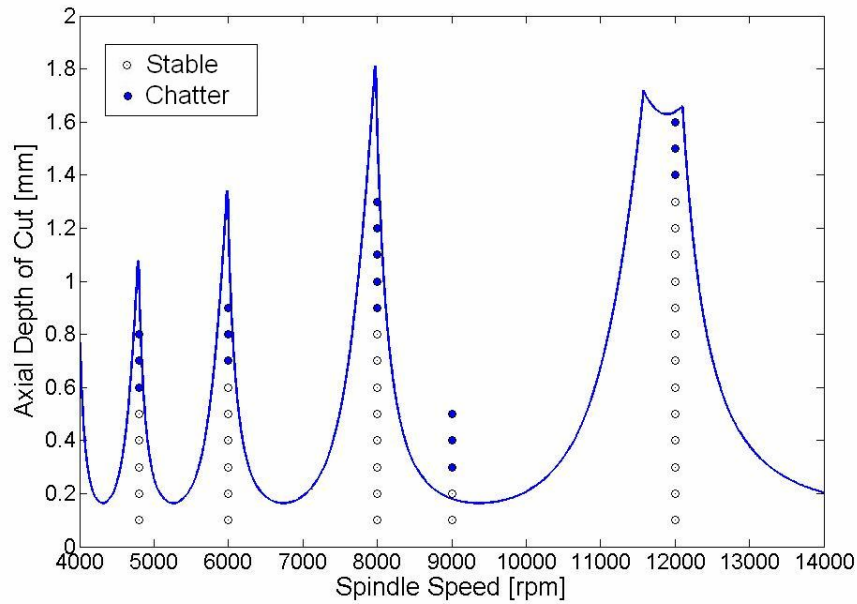


Figure 18. Experimental and predicted stability limits for down milling of aluminum test piece using 60 mm tool overhang length and 3 mm radial depth.

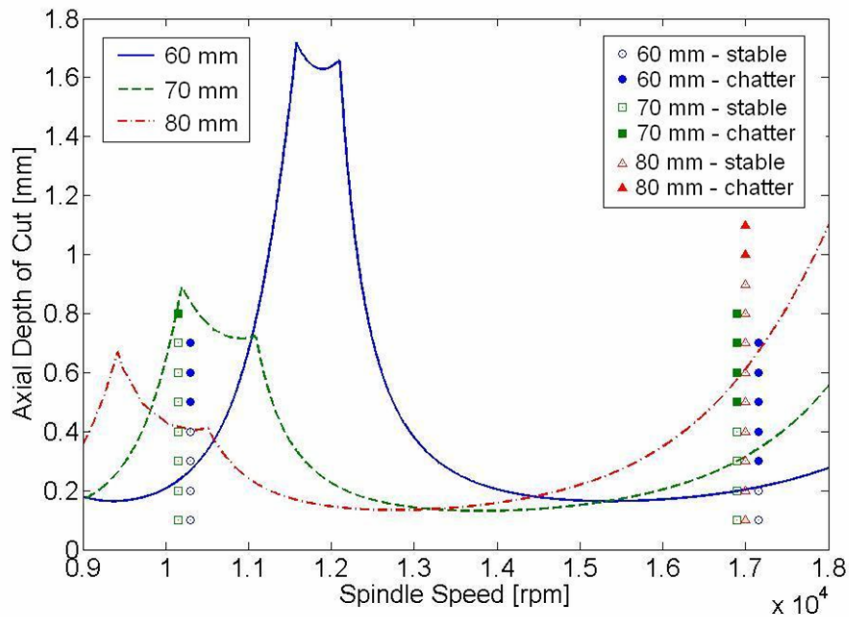


Figure 19. Experimental and predicted stability limits for milling of aluminum test piece using 60 mm, 70 mm and 80 mm tool overhang lengths resulting in high stability lobes at different speed zones.

As a second stability prediction application, the effect of the tool overhang length change on the stability diagram is considered. The tool overhang length may be changed due to operational requirements, or to modify the stability diagram to increase the stable depths at certain speeds. The model presented can be used for both cases. Figure 19 shows stability diagram for 3 different tool overhang lengths: 60, 70 and 80 mm for the same cutting conditions used in the previous application. Again, the analytical method was used for the prediction of tool point FRF which was utilized in the analytical milling stability model together with the experimentally identified force coefficients for the generation of the diagrams. Note that due to the analytical FRF model, the prediction of the new FRFs for the new tool lengths is very fast and does not require additional testing. Figure 19 shows that 60 mm tool overhang length results in very large stability lobe around 12000 rpm. However, if the maximum spindle speed available on the spindle is less than this, say 10000 rpm, then this lobe cannot be utilized. Moreover, this tool length results in a very low stability limit at around 10000 rpm as shown in the diagram. Contrary to what one might expect intuitively, increasing the tool overhang length 10 mm to 70 mm produces a much higher stability pocket at this speed, and the depth of cut can be increased from 0.2 mm to 0.8 mm resulting in a substantial productivity gain. A similar problem arises if the process is to be carried out at a much higher spindle speed, say at 17000 rpm, if it is available on the machine. As it can be seen from the diagram, 60 mm tool overhang length again results in a very low stable depths at those speeds. However, unlike the previous case of 10000 rpm, 70 mm tool overhang length does not produce much higher stability limits in this speed zone. In this case, increasing the tool overhang length another 10 mm to total of 80 mm produces much larger stability limits for those high speeds, resulting in about 3 folds amplification in the stable material removal rate. These predicted results are verified by chatter tests, and as shown in Figure 19 the agreement between the experiments and the predictions is quite acceptable. Thus, it can be concluded that the integration of the analytical FRF and stability predictions can be a strong tool for a virtual machining environment where the stable and optimal conditions can be identified with minimal amount of testing.

6. CHATTER SUPPRESSION BY NOISE MEASUREMENTS

In this section the practical determination of the locations of the high stability zones are discussed. There are mainly two areas in the stability analysis of machining operations where noise measurements can be used. The use of noise measurements for the suppression of chatter are rather different than the regular stability analysis. In this case nothing is known about the dynamic system and the objective is to obtain the maximum stable depth of cut by just measuring the noise during cutting. Since no parameter about the cutting system needs to be known, the only measurement device needed is a microphone and a data acquisition setup. In this case the meaning of equation (13-14) and (ε) become important. First of all it must be mentioned here that ε can be assumed to be close to zero at the intersection points of the lobes. The chatter frequency varies with spindle speed resulting in variation of the phase angle (ε) as well. The phase becomes close to zero at the intersection of the lobes, i.e. at the peaks of the stability pockets. In fact this is the reason why high stability is obtained at those locations since the phase is the driving force behind chatter. As presented above, the highest stable depth of cut can be found at the pocket of the first lobe. Therefore, equation (14) becomes as follows by substituting $\varepsilon=0$ and $k=1$:

$$n = 60\omega_c / N \quad (81)$$

Therefore, the location of the first lobe's pocket, i.e. the highest stability zone, can be obtained provided that the chatter frequency is measured. In practice, the methodology discussed above is applied as follows. Assume that there is chatter for a given milling operation and the dynamic system has one dominant mode. If the chatter frequency is obtained by measuring the sound during cutting, a new spindle speed can be calculated using equation (81). Then, cutting is repeated with the same depth of cut using the new spindle speed. If the new cutting operation is stable then the pocket is found and higher depths of cut can be tried for the same spindle speed. However, if there is still chatter in the process and the new calculated spindle speed by the measured chatter frequency is the same as the one used, then the depth of cut is higher than the maximum possible stable depth of cut, i.e. the stability limit. It means that we have found the spindle speed corresponding to the first pocket, but the depth of cut is higher than the limit. Thus, search for the stable depth is continued by trying

smaller depth of cuts. There may be cases where two modes of the system are comparable and the stability behaviour may not be as smooth as that of a one degree of freedom system. In such cases the corresponding mode of the measured chatter frequency is not known which may cause difficulties in determining the location of the first pocket and the highest possible stable depth of cut. In this situation, calculating a new spindle speed value may yield incorrect pocket positions. If the detected chatter frequency at the new spindle speed is quite different from the initial one, and if this chatter frequency was not observed in the previous test, then instead of calculating a new pocket location, the depth of cut should be decreased at this spindle speed looking for the stability limit. In some extreme cases, the measured chatter frequency may be due to the higher harmonics of the dynamic system which is different from the most flexible mode in the first run. Then, the calculated spindle speed will again give incorrect pocket positions. In all those cases there will be chatter for all iteratively calculated spindle speeds. Therefore, the stable depth of cut should be decreased and the iterations must be continued as proposed above.

6.1. Example applications

Two different experimental cases are presented in this section in order to show the application of the previously discussed approaches. In the first experiment, the stability diagram obtained by analytically calculated FRFs is verified, whereas in the second case the stability limit of a different cutting process is obtained by just noise measurements during cutting. In both experimental cases a high speed, 5-axis vertical machining center was used which has a maximum of 18000 rpm spindle speed. A 4-fluted coated carbide milling tool with 12 mm diameter was used to mill AISI 1050 steel. An impact hammer and an accelerometer for modal testing, and a sound setup that consists of a microphone and a data acquisition system are used for measurements. In the first experimental case, the FRF at the tool tip of the CNC machine is calculated by the analytical receptance coupling method described in Section 5. The tool having an overhang length of 55 mm was clamped to the power chuck type tool holder. The analytical results along with the modal test results can be seen in Figure 20. In cutting tests, the radial depth of cut was selected as 2 mm and the feed rate per tooth used during the tests was 0.05 mm/rev. By using the calculated FRFs, the stability diagram of the system is obtained as shown in Figure 21 along with the experimental results and example surface finishes for both stable and unstable cuts. Firstly, from the measured sound data (see Figures 21.b and 21.c) the tooth passing frequencies can be noticed, which can be calculated as follows:

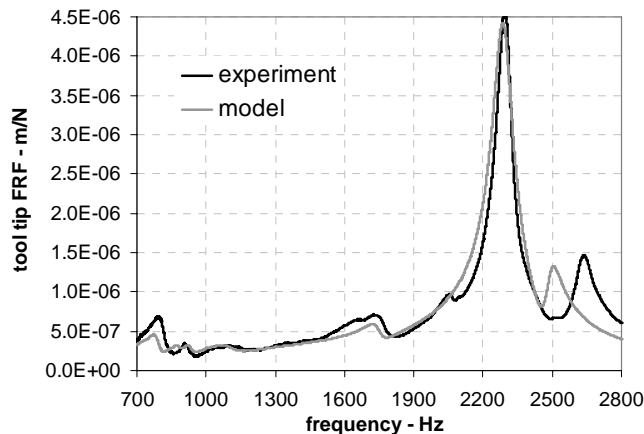


Figure 20. The comparison of the calculated FRFs with the measured ones.

$$\omega_{tooth_passing} = \frac{\omega_c}{60N_k} \quad N_k = 1,2,3,4 \quad (82)$$

Considering the 17000 rpm tests, the chatter is expected to be dominated by the second most flexible mode of the dynamic system. As can be seen from Figure 21.c the measured chatter frequency is very close to the second mode's natural frequency verifying our approach. Another interesting observation from that test is the existence of the other harmonics that are excited. This is mainly because of the fact that the selected depth of cut is higher than the stability limit. If the depth were equal to the

stability limit, i.e. 3.8 mm, than in the frequency measurements less frequency content would be seen, and the dominant one would be very close to the natural frequency of the second most flexible mode. However, in milling due to the rotation of the cutter which introduces higher harmonics of the tooth passing frequency, the sideband frequencies defined as the addition and subtraction of integer multiples of the tooth frequency to and from the chatter frequency, will come into the picture as well [7]. Depending on the radial depth of cut which controls the strength of the Fourier components, more frequency content may be present. For small depth of cuts, the higher Fourier components of the time varying-periodic directional coefficients are necessary resulting in higher frequency content in the response as well [7]. The higher harmonics that are measured can be seen in Figure 21.c (3968 Hz) which is equal to the sum of the tooth passing frequency (1133 Hz) and chatter frequency (2834 Hz). The predicted stability lobes and experiments are observed to be in good agreement.

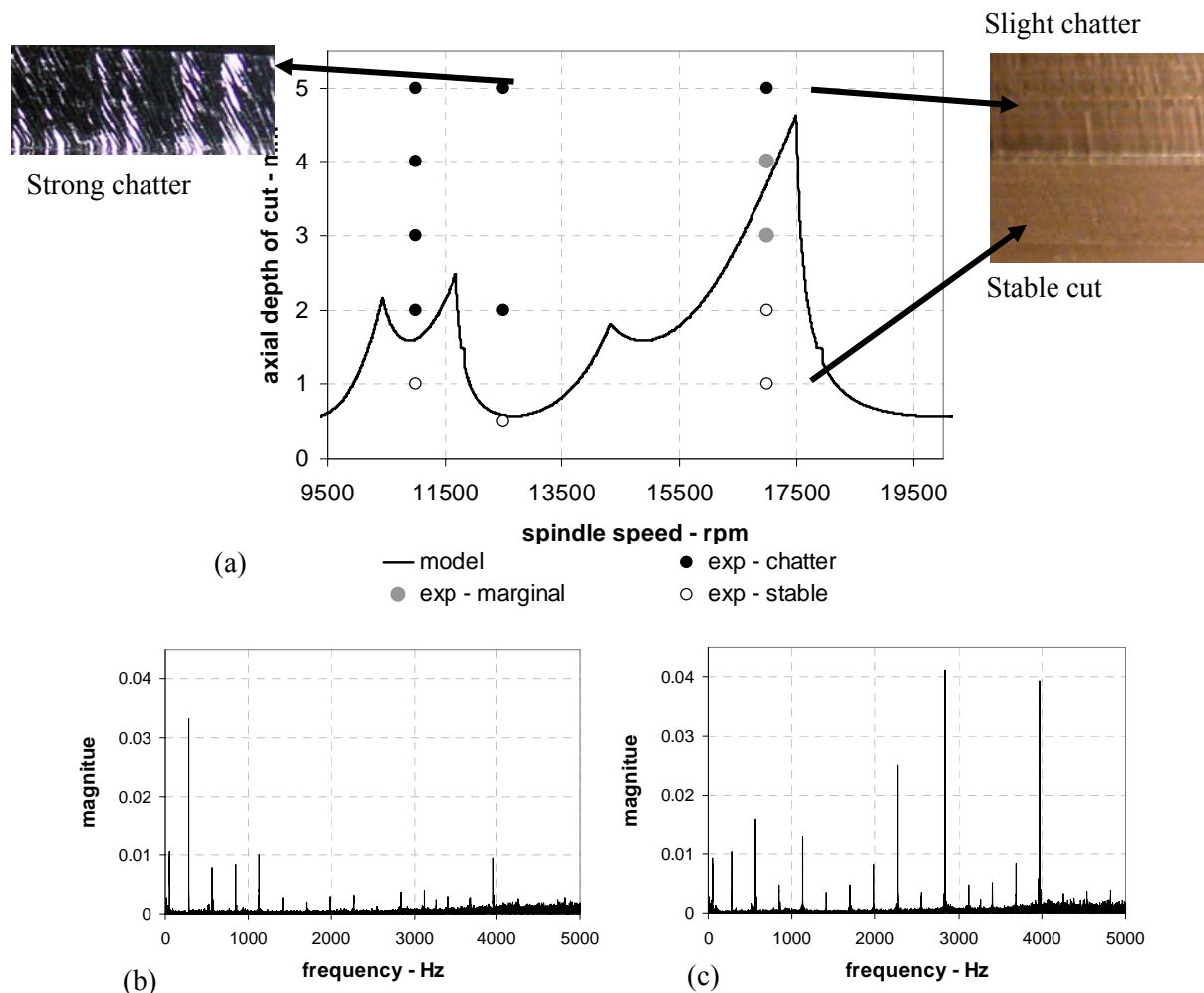
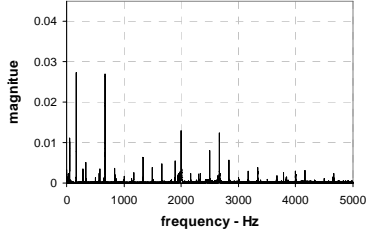
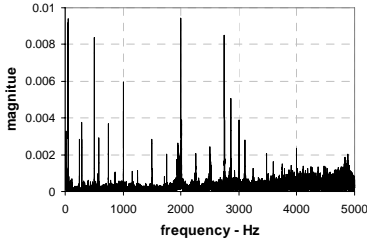
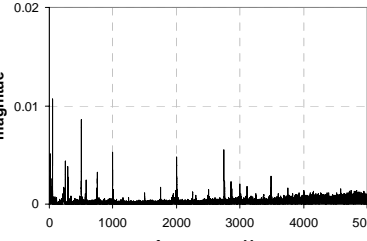
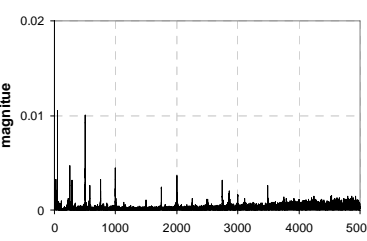
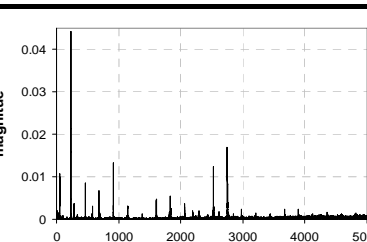
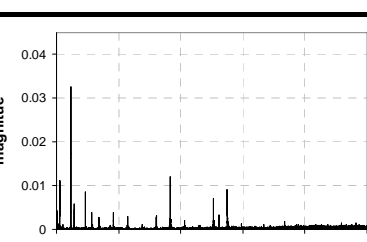


Figure 21. (a) Analytically calculated stability diagram and the experiment results with surface finishes, and FFT spectrum of the measured sound data for the tests at 17000 rpm for the axial depth of (b) 1 mm and (c) 5 mm.

In the second experiment case, the tool is clamped with an overhang length of 65 mm and the radial depth of cut is selected as 3 mm. No measurement or analytical calculation is done in order to obtain the FRF of the dynamic system. The aim was to calculate the location of the possible stability pockets by just measuring the chatter frequency. However it should be mentioned here that, the absolute stability limit is roughly estimated to be around 0.2 mm by using the results of the first case above. Also the finished surface is observed by naked eye for the decision of the chatter during the cut. The initial test point is selected to be at 10000 rpm and 1 mm axial depth. The test data can be found in Table 3. As can be seen from the FFT spectrum of the sound measurement of Test 1, excluding the peaks at tooth passing frequencies, basically two modes are excited at 2000 Hz and 2670 Hz, and

Table 3. Sound measurement results for the second experiment set.

Test No	Spindle speed (rpm)	Axial depth (mm)	Chatter?	Chatter Frequency (Hz)	FFT spectrum of the measured sound data
1	10000	1	YES	2000 and 2670	
2	15000	1	YES	2000 and 2750	
3	15000	0.6	LIMIT	2000 and 2750	
4	15000	0.3	NO		
5	13750	1	YES	2750	
6	13750	0.6	NO		

from the finished surface it is decided that there was chatter. At this moment it is clear that there are two dominating modes at the dynamic system. Therefore, two different spindle speeds are calculated by using equation (81) i.e. 15000 rpm for 2000 Hz for the second pocket and 13500 rpm for 2670 Hz for the third pocket. The pockets are selected so that the calculated spindle speeds are in the range of the maximum spindle speed of the CNC that is used during tests. After this point it is known that there are possible pocket locations. 15000 rpm is selected for the first trial. The results of these tests can be seen in Table 3 (tests no 2-4). The axial stable depth is found to be 0.3 mm whereas the limiting stable depth of cut is found to be around 0.6 mm. It can be seen from these experimental results that the chatter frequency was dominated by the mode around 2000 Hz which was the chatter frequency that is used to calculate this spindle speed. In order to search for higher stability limits the second possible pocket position at 13750 rpm is considered for the next run. The results of these sets can be seen in Table 3 i.e. tests 5 and 6. This time the stable depth of cut is obtained at 0.6 mm axial depth of cut. And the limiting depth of cut is found to be around 0.8 mm. Also the dominant mode at the chatter is measured to be 2750 Hz which was expected.

7. CONCLUSION

High productivity and quality in machining strongly depend on the process dynamics and stability. Rigidity of machine tools and selection of process parameters are two main factors in dynamic behavior of cutting operations. In this paper, methods that can be used for analysis and modeling of machine tool structures and cutting process stability are reviewed. These methods can be used to analyze as well as improve the dynamic behavior of machining processes. Perhaps the most important application of these methods is the analysis and suppression of the chatter which is the most critical vibration type for machining systems. The analytical methods and suppression techniques presented here can be used to improve stability and productivity of the machining operations. The selected and presented methods have been applied, and are currently being used in industry. The results observed so far indicate that the dynamics in cutting is a complicated problem, but substantial advancements can be obtained using modeling. Therefore, the work in this area is expected to continue in the coming years.

8. REFERENCES

- [1] J. Tlustý; J. Poláček.; M. Poláček, The Stability of Machine Tools against Self Excited Vibrations in Machining, ASME International Research in Production Engineering, 465-474, 1963.
- [2] S.A. Tobias, Machine Tool Vibration, Blackie and Sons Ltd., 1965.
- [3] J. Tlustý, Manufacturing Processes and Equipment, Prentice Hall, Upper Saddle River, NJ, 2000.
- [4] I. Minis, T. Yanushevsky, R. Tembo, R. Hocken, Analysis of Linear and Nonlinear Chatter in Milling, Annals of the CIRP, 39, 459-462, 1990.
- [5] I. Minis; T. Yanushevsky, A New Theoretical Approach for the Prediction of Machine Tool Chatter in Milling, Trans. ASME Journal of Engineering for Industry 115, 1-8, 1993.
- [6] Y. Altintas, E. Budak, Analytical Prediction Of Stability Lobes In Milling, Annals of the CIRP, 44 (1), 357-362, 1995.
- [7] E. Budak, Y. Altintas, Analytical Prediction of Chatter Stability in Milling - Part I: General Formulation, Part II: Application To Common Milling Systems, Trans. ASME Journal of Dynamic Systems, Measurement and Control, 120, 22-36, 1998.
- [8] M.A. Davies, J.R. Pratt, B. Dutterer, T.J. Burns, Stability Prediction of Low immersion Milling, Trans. ASME Journal of Manufacturing Science and Engineering, 124, 217-225, 2002.
- [9] T. Insperger, B.P. Mann, G. Stephan, P.V. Bayly, Stability of Up-Milling and Down-Milling, Part I: Alternative Analytical Methods, International Journal of Machine Tools and Manufacture, 43, 25-34, 2003.
- [10] S.D. Merdol, Y. Altintas, Multi Frequency Solution of Chatter Stability Limits for Low Immersion Milling, Trans. ASME Journal of Manufacturing Science and Engineering, 126, 459-466, 2004.
- [11] W.T. Corpus, W.J. Endres, Added Stability Lobes in Machining Processes That Exhibit Periodic Time Variation, Part 1: An Analytical Solution. Part 2: Experimental Validation, Trans. ASME Journal of Manufacturing Science and Engineering, 126, 467-480, 2004.
- [12] Kaneko, T., Sato, H., Tani, Y., O-hori, M., Self-Excited Chatter and its Marks in Turning, Transactions of ASME, 222, 106-228, 1984.
- [13] Minis, I. E., Magrab, E. B., Pandelidis, I. O., Improved Methods for the Prediction of Chatter in Turning Part 3: A Generalized Linear Theory, Transactions of ASME, 112, 12-20, 1990.

- [14] Rao, C. B., Shin, Y. C., A Comprehensive Dynamic Cutting Force Model for Chatter Prediction in Turning, *International Journal of Machine Tools & Manufacture*, 39, 1631-1654, 1999.
- [15] Atabey, F., Lazoglu, I., Altintas, Y., Mechanics of Boring Processes – Part I, *International Journal of Machine Tools & Manufacture*, 43, 463-476, 2003.
- [16] Lazoglu, I., Atabey, F., Altintas, Y., Dynamic of Boring Processes: Part III – Time Domain, *International Journal of Machine Tools&Manufacture*, 42, 1567-1576, 2002.
- [17] Budak, E. and Ozlu, E., Analytical Modeling of Chatter Stability in Turning and Boring Operations: A Multi-Dimensional Approach, *Annals of the CIRP*, Vol. 56, 2007.
- [18] Ozlu, E. and Budak, E., Analytical Modeling of Chatter Stability in Turning and Boring Operations Part I: Model Development- Part II: Experimental Verification, *Trans. ASME Journal of Manufacturing Science and Technology*, August 2007.
- [19] Altintas, Y., *Manufacturing Automation*, Cambridge University Press, 2000.
- [20] T. Schmitz, R. Donaldson, Predicting High-speed Machining Dynamics by Substructure analysis, *Annals of the CIRP*, 49(1), 303-308, 2000.
- [21] T. Schmitz, M. Davies, M. Kennedy, Tool Point Frequency Response Prediction for High-speed Machining by RCSA, *Journal of Manufacturing Science and Engineering* 123, 700-707, 2001.
- [22] A. Ertürk, H.N. Özgüven, E. Budak, Analytical Modeling of Spindle-Tool Dynamics on Machine Tools Using Timoshenko Beam Model and Receptance Coupling for the Prediction of Tool Point FRF, *International Journal of Machine Tools and Manufacture*, 46, 1901-1912, 2006.
- [23] E. Budak, A. Ertürk, H.N. Özgüven, A Modeling Approach for Analysis and Improvement of Spindle-Holder-Tool Assembly Dynamics, *Annals of the CIRP*, 55, 369-372, 2006.
- [24] A. Ertürk, H.N. Özgüven, E. Budak, Effect Analysis of Bearing and Interface Dynamics on Tool Point FRF for Chatter Stability in Machine Tools by Using a New Analytical Model for Spindle-Tool Assemblies, *International Journal of Machine Tools and Manufacture*, 47(1), 23-32, 2007.
- [25] Ertürk, A., Budak, E., Ozguven, H.N., Selection of Design and Operational Parameters in Spindle-Holder-Tool Assemblies for Maximum Chatter Stability by Using a New Analytical Model, *International Journal of Machine Tools and Manufacture*, 47, 1401-1409, 2007.
- [26] T. Delio, J. Tlustý, S. Smith, Use of Audio Signals for Chatter Detection and Control, *Trans. ASME, Journal of Engineering for Industry*, 114, 146–157, 1992.
- [27] S. Smith, J. Tlustý, Stabilizing Chatter by Automatic Spindle Speed Regulation”, *Annals of the CIRP*, 41(1), 433–436, 1992.
- [28] E. Özlü , O. Özşahin , E. Budak, H. N. Özgüven, The Use of Noise Measurements in Machining Stability Analysis, *Proceedings of the Inter-Noise Conference, Istanbul, Turkey*, 2007.
- [29] Budak, E., Analytical Methods for High Performance Milling-Part II: Process Dynamics and Stability, *International Journal of Machine Tools and Manufacture*, 46, 1489-1499, 2006.
- [30] Slavicek, J., The Effect of Irregular Tooth Pitch on Stability of Milling, *Proceedings of the 6th MTDR Conference, Pergamon Press, London*, 15-22, 1965.
- [31] Opitz, H., Dregger, E.U. and Roese, H., Improvement of the Dynamic Stability of the Milling Process by Irregular Tooth Pitch, *Proceedings of the Adv. MTDR Conference, No.7*, 213-227, 1966.
- [32] Vanherck, P., Increasing Milling Machine Productivity by Use of Cutters with Non-Constant Cutting Edge Pitch", 8th MTDR Conference, Manchester, 947-960, 1967.
- [33] Altintas, Y., Engin, S. and Budak, E., Analytical Stability Prediction and Design of Variable Pitch Cutters, *Trans. ASME, Journal of Manufacturing Science and Engineering*, 121, 173-178, 1999.
- [34] Budak, E., An Analytical Design Method for Milling Cutters with Non Constant Pitch to Increase Stability-Part I: Theory- Part II: Application, *Trans. ASME Journal of Manufacturing Science and Engineering*, Vol. 125, pp. 29-38, 2003.
- [35] Budak, E., Improvement of Productivity and Part Quality in Milling of Titanium Based Impellers by Chatter Suppression and Force Control, *The Annals of the CIRP*, 49/1, 31-36, 2000.
- [36] Budak, E., Altintas, Y. , Armarego, E.J.A., Prediction of Milling Force Coefficients From Orthogonal Cutting Data, *Trans. ASME Journal of Manufacturing Science and Engineering*, 118, 216-224, 1996.
- [37] Merdol, S.D. and Altintas, Y., Multi Frequency Solution of Chatter Stability Limits For Low Immersion Milling, *Trans. ASME Journal of Manufacturing Science and Engineering*, 126, 459-466, 2004.
- [38] Weck, M., Altintas, Y. and Beer, C., CAD Assisted Chatter Free NC Tool Path Generation in Milling, *International Journal of Machine Tools and Manufacture*, 34, 879-891, 1994.

